VOL. 17 No. 7-8, pp. 189-232 JANUARY-FEBRUARY 1956

Philips Technical Review

DEALING WITH TECHNICAL PROBLEMS
RELATING TO THE PRODUCTS, PROCESSES AND INVESTIGATIONS OF
THE PHILIPS INDUSTRIES

EDITED BY THE RESEARCH LABORATORY OF N.V. PHILIPS' GLOEILAMPENFABRIEKEN, EINDHOVEN, NETHERLANDS

THE "SCENIOSCOPE", A NEW TELEVISION CAMERA TUBE

by P. SCHAGEN, J. R. BOERMAN, J. H. J. MAARTENS and T. W. van RIJSSEL.

621.383.2:621.385.832:621.397.611

The image iconoscope is a television camera tube with one or two notable advantages: the picture quality is very good, the tube is not very much affected by stray electric or magnetic fields, and the field of vision can be varied electrically. On the other hand, the sensitivity of this tube is not as high as is desirable for many practical applications. Accordingly, an investigation was made with the aim of designing another camera tube which would combine the above-mentioned advantages with higher sensitivity. These efforts have resulted in a new type of camera tube, the "Scenioscope", which in many respects, is similar to the image iconoscope in design. Its operation, however, is altogether different and it therefore merits a new name. This new tube is so sensitive as to give an acceptable, though not entirely noise-free, picture with an object illumination of only 100 lux, and an excellent picture almost entirely free from noise with 300 lux.

Introduction

A few years ago, two articles on the image iconoscope 5854, a television camera tube designed in the Philips laboratories, were published in this Review [1][2]. This tube has a number of very valuable features, particularly its excellent picture quality with adequate scene illumination, and its facility for continuous variation of the field of vision by purely electrical means.

The disadvantage of the image iconoscope, on the other hand, is that the picture quality deteriorates when the illumination level drops below roughly 1000 lux. This is mainly owing to increasing interference from spurious signals (see later). Compensation is possible to some extent, by line-by-line clamping of the black level [3], which largely suppresses the spurious signals superimposed on the picture signal and thus leaves the received picture — at least that side of it at which scanning begins — almost free from this type of interference.

Although the picture quality at low illumination levels is very much improved by this periodic clamping of the black level, it is nevertheless inadvisable to take the illumination very far below 400-500 lux; apart from a renewal of interference from residual spurious signals in the line direction, the picture is also affected by *noise* (mainly due to the first amplifier valve in the camera pre-amplifier).

Although an illumination level between 1000 and 1500 lux is readily procured in a television studio, it is associated with a heat output high enough to cause discomfort to the performers. Also, in the televising of stage productions, flood-lit sports, and so on, the installation of special extra lighting for the occasion involves major problems. To transmit such programmes, then, European television stations often employ the *image orthicon*, which is the camera tube employed throughout the United States. However, the picture quality of this more sensitive tube is in some respects inferior to that of the image iconoscope when the latter is operated at an adequate illumination level. Attempts have therefore been made everywhere to develop a more sensitive camera tube, based on the image iconoscope and retaining the high quality of its picture.

[1] P. Schagen, H. Bruining and J. C. Francken, Philips tech. Rev. **13**, 119-133, 1951/52.
[2] J. C. Franken and H. Bruining, Philips tech. Rev. **14**, 327-335, 1952/53.
[3] See e.g.: P. Schagen, T. Ned. Radiog. **16**, 236 etc., 1951, and "On the image iconoscope, a television camera tube", Thesis, Vrije Universiteit, Amsterdam 1951, page 58 etc.; H. Bruining, Le Vide **7**, 1255, 1952; J. Haantjes and Th. G. Schut, Philips tech. Rev. **15**, 300, 1953/54.

In England, these experiments produced the "P.E.S. Photicon" (or "photo-electrically stabilized Photicon") [4]) known in Germany as the "Riesel-Ikonoskop" [5]), and in the Philips laboratories at Eindhoven a tube known as the "Scenioscope" (*fig. 1*). Despite a superficial similarity in principle

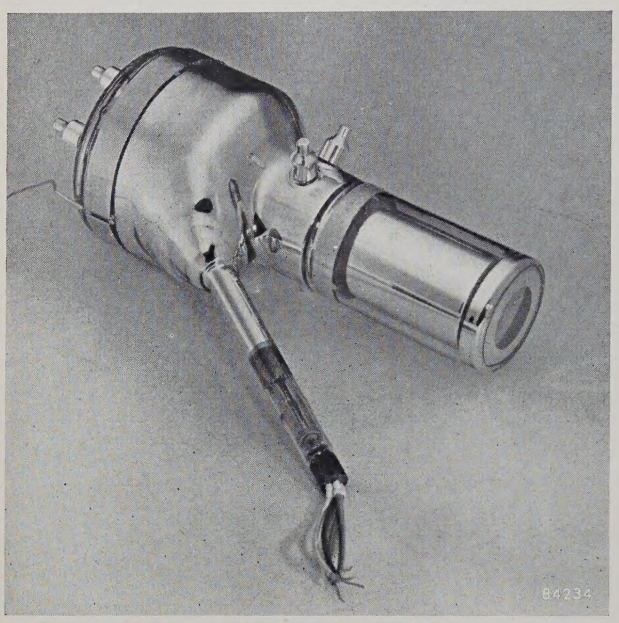

Fig. 1. The "Scenioscope" (identical in appearance with the image iconoscope type 5854). The photo-cathode is on the right, and the arm of the electron gun producing the scanning beam projects into the foreground.

between the P.E.S. photicon and the "Scenioscope" the two are entirely different in design. The "Scenioscope" is more sensitive and, at the same time, much simpler.

The operation of the "Scenioscope", which is identical in appearance to the image iconoscope 5854, will now be explained and its characteristics compared with those of the image iconoscope.

The image iconoscope

Preparatory to explaining the operation of the "Scenioscope" let us consider one or two of the principal features of the image iconoscope as described in article [1]). An image of the scene to be televised is formed, by a special lens, on a transparent photo-cathode (*fig. 2*). The photo-electrons emitted by this cathode are deflected by two fields, one electric and one magnetic, so as to strike points on a mica target corresponding to the image points from which they were emitted, thus producing on the target a pattern or "image" of positive charges, which is then scanned by an electron beam. As they are scanned one after another, the individual picture elements assume a potential which corresponds to a secondary-emission factor of unity. This equilibrium potential is slightly higher than the potential of the collector (that is, the earthed metal coating inside the bulb; the potential of the photo-cathode is —1000 V). Now, between consecutive scannings, the potential of the individual target elements drops, owing to the fact that they intercept slow secondary electrons released from other points on the target by the fast photo-electrons and the equally fast electrons of the scanning beam; this interception effect is known as *redistribution*. The probability that the secondary electrons released from a particular target element by the photo-electrons will escape to the collector or to other parts of the target increases as the above-mentioned potential decreases. Hence the effective secondary-emission factor δ_{eff}, or average number of secondary electrons that can escape from the target per incident primary photo-electron, increases; thus the photo-electrons contribute more and more to the charge pattern on the target. To illustrate this point, *fig. 3a* shows δ_{eff} plotted against the potential of a target element. Similarly, fig. 3*b* shows the variation of the potential of an element as a function of the time constituting one complete frame period τ (i.e. 1/25 second in European television

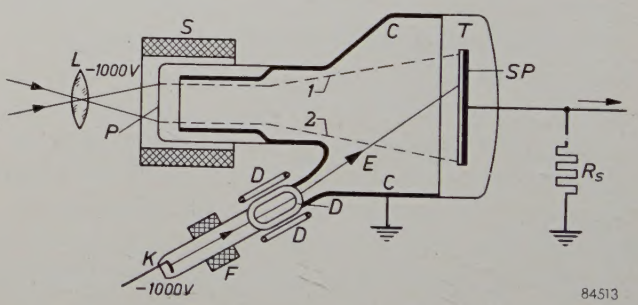

Fig. 2. Schematic cross-section of the image iconoscope. *L* lens; *P* photo-cathode; *S* coil of the magnetic electron lens; *T* target (mica); *C* collector; *E* scanning beam supplied by an electron gun of which only the cathode *K* is shown in the diagram; *F* focusing coil; *D* deflecting coils; *SP* signal plate; R_s signal resistor.

systems), with and without illumination, V_0'' and V'_0 representing respectively the potentials of the particular element at the end of period τ; the difference $V_0''-V_0'$ governs the contribution of the element to the video signal.

For an image iconoscope operating ideally, each photo-electron should produce on the target a

[4]) J. E. Cope, L. W. Germany and R. Theile, Improvements in design and operation of image iconoscope type camera tubes, J. Brit. Inst. Rad. Engrs. **12**, 139-149, 1952.

[5]) R. Theile, Die Signalerzeugung in Fernseh-Bildabtaströhren, Arch. elektr. Übertragung **7**, 15-27, 281-290 and 328-337, 1953.

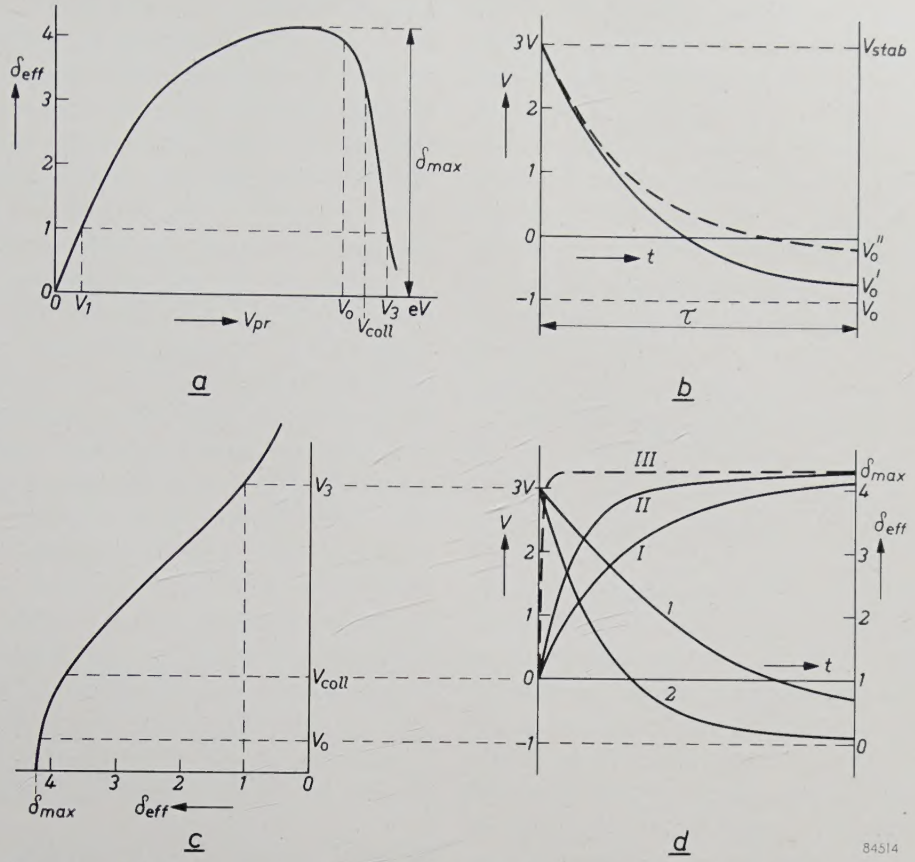

Fig. 3. *a*) Effective secondary emission factor (δ_{eff}) of an insulator, plotted against the energy (V_{pr}) of the primary electrons. $\delta_{eff} = 1$ when $V_{pr} = V_1$ or $V_{pr} = V_3$. Potential V_3 is one or two volts higher than the collector potential V_{coll}. V_0 is the potential at which the flow of secondary electrons to the particular target element is completely cut off.
b) Potential V of a target element in the image iconoscope, plotted against the time t, in the frame period τ between two scannings. Full curve: photo-cathode not illuminated; dotted curve: photo-cathode illuminated. Both curves start at the equilibrium potential V_{stab} ($\approx V_3$, see *a*) and approach V_0 asymptotically. By the end of interval τ, V drops to V_0' or V_0'' respectively. The contribution to the output signal is $V_0''-V_0'$.
c) Right-hand part of the curve shown in *a*, rotated 90°, showing relation to *d*), where *1* and *2* are $V = f(t)$ curves like the full curve in (*b*). From *1* we derive, with the aid of (*c*), curve *I* for $\delta_{eff} = f(t)$, and from *2* curve *II*. Curve *2*, sloping downward more steeply than *1*, produces higher values of δ_{eff} (*II* is above *I*, that is, closer to the ideal curve *III*), and is therefore more favourable than *1*.

positive picture charge of magnitude $(\delta_{max}-1)e$, where δ_{max} is the maximum value attainable by δ_{eff} (fig. 3*a*), and e is the charge on the electron. The signal current output of the tube would then be roughly 1.3 ($\delta_{max}-1$) times the photo-current corresponding to the brightest parts of the picture; the factor of 1.3 is included to allow for the fact that although the photo-current is continuous, the video current flows only 75% of the time, owing to the line and frame suppressions.

In reality, however, the signal current remains very much smaller, for two reasons. Firstly, immediately after a scanning, the secondary-emission factor δ_{eff} differs only slightly from unity, and afterwards rises only gradually (fig. 3*d*, curves *I* and *II*). Secondly, it is precisely the potential of the most brightly "illuminated" target elements that drops the least (fig. 3*b*): therefore the δ_{eff}

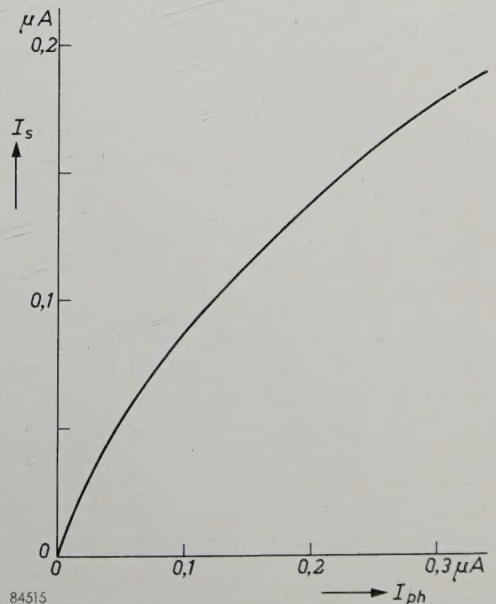

Fig. 4. Signal current I_s plotted against photo-current I_{ph} for image iconoscope 5854.

of these elements invariably falls short of the maximum. Although δ_{max} in image iconoscope 5854 is roughly 4, which gives rise to a maximum signal current 1.3 $(4-1) \approx 4 \times$ the photo-current, it is found in practice that, owing to the above-mentioned effects, the maximum video current is at most roughly equal to the photo-current at low illumination levels. Moreover, with an increasing light level the effect of the consequent increase in photo-current becomes smaller and smaller, so that the characteristic of the image iconoscope (signal current against photo-current) bends in the manner shown in *fig. 4*, with a "gamma" smaller than unity.

Possible methods of increasing the sensitivity

That the actual sensitivity of the image iconoscope is appreciably lower than the ideal sensitivity apparently arises from the fact that the potential of the target elements *drops too slowly* to enable the photo-electrons to contribute their utmost to the construction of the potential image immediately after a scanning (fig. 3*d*). If this drop in potential could be accelerated, a stronger signal could be obtained. There are three possible methods of accelerating the drop, i.e.:

1) intensifying the redistribution effect;
2) flooding the target with low-velocity electrons;
3) dissipating the charge by conduction.

They will now be discussed one by one.

Intensifying the redistribution effect

The drop in potential already referred to is caused by redistribution (that is, the interception of low-velocity electrons released by secondary emission from other parts of the target). It is therefore reasonable to suppose that the sensitivity can be increased by increasing the number of redistribution electrons; this can be done, for example, by increasing the scanning current (*fig. 5*). In fact this method does produce a stronger signal [6]), provided that the scanning current is not taken above a certain limit. Beyond this limit, however, the signal strength diminishes again owing to the fact that the erasing of positive video charges, accumulated at the "illuminated" points on the target, becomes more and more intensive as the number of redistribution electrons increases. Another disadvantage is that the spurious signals also become stronger as the number of redistribution electrons increases (a spurious signal, or "shadow signal", may be defined as a signal produced by a camera tube without illumination, and visible on the picture tube of the receiver — for example, the bottom right-hand corner of the screen appearing brighter than the top left-hand corner. It arises mainly from a lack of uniformity of redistribution over the target elements; see article [1])).

Intensifying the redistribution effect does not therefore greatly improve matters.

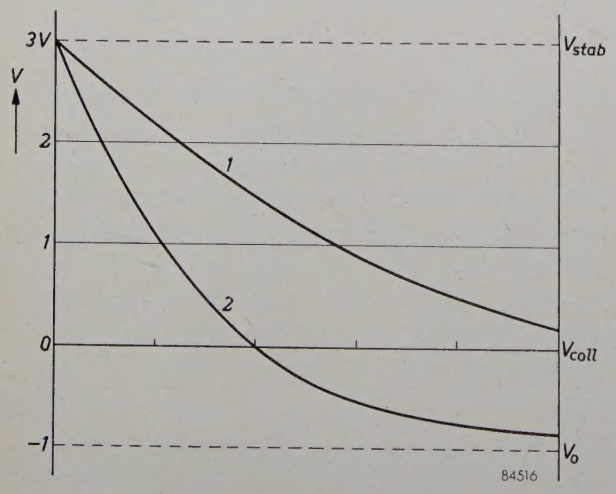

Fig. 5. $V = f(t)$ curves (*1* and *2*) for a non-illuminated image iconoscope, *2* referring to a heavier scanning current than *1*.

Flooding with low-velocity electrons

In England, the "P.E.S. Photicon" is based on the flooding of the target with low-velocity electrons, a method already suggested [7]) in 1934 as a means of improving the ordinary iconoscope. The effect of such flooding is very much the same as that of increasing the number of redistribution electrons, that is, it accelerates the drop in potential of the target elements. However, the advantage of flooding is that it does not increase, and may even reduce, the strength of the spurious signals. Variable-bias auxiliary electrodes arranged all round the target enable the low-velocity electrons to be directed to the parts of the target where redistribution electron concentration is lowest.

In the "P.E.S. Photicon", flooding with low-velocity electrons is achieved with the help of a transparent auxiliary photo-cathode applied to the inside of the bulb and maintained at collector potential (see articles referred to in notes [4]) and [5])). Incandescent lamps arranged around the tube enable the photo-cathode illumination and therefore the "rain" of low-velocity electrons (whence the German name: "Riesel-Ikonoskop") to be varied

[6]) P. Schagen, On the mechanism of high-velocity target stabilization and the mode of operation of television camera tubes of the image-iconoscope type, Philips Res. Rep. **6**, 135-153, 1951.

[7]) A. W. Vance and H. Branson, U.S. Patent 2 147 760, of 1934.

as required. A schematic cross-section of the "P.E.S. Photicon" is shown in *fig. 6*.

The gain in sensitivity procured in this tube is mainly attributable to the almost complete elimination of spurious signals, enabling a good-quality picture to be obtained at a lower illumination level

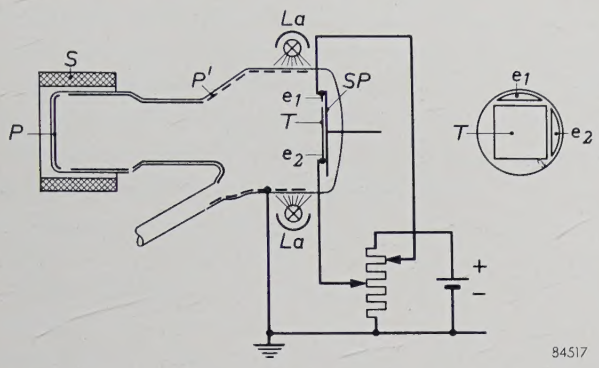

Fig. 6. Schematic cross-section of a "P.E.S. Photicon" (reproduced from fig. 7, page 145, of the article referred to in note [4]). P' auxiliary photo-cathode, illuminated by a ring of incandescent lamps *La*. Segment-shaped control electrodes e_1 and e_2 with variable voltage, direct the low-velocity photo-electrons from P' to parts of the target plate T where the concentration of redistribution electrons is low. This suppresses the spurious signals. Meanings of the other letters as in fig. 2.

than with the ordinary image iconoscope, subject to a limit imposed by noise. It is stated in the literature [8]) that the practical gain in sensitivity as compared with the ordinary image iconoscope is roughly a factor of 2.

In principle, the sensitivity could probably be increased a little more by augmenting the current of low-velocity electrons and reducing the potential of the auxiliary photo-cathode slightly in relation to that of the collector; this would enable the potential of the target elements to drop still lower (i.e. to below the value V_0 at which the flow of secondary electrons to the target element is suppressed, see fig. 3*b*). However, practical experience has shown that under these conditions it is impossible to control the electrons (with the auxiliary electrodes referred to) so as to avoid spurious signals. Moreover, it is evident that the low-velocity electrons proceed preferentially to the "brightest" parts of the target, where the potential is highest; this likewise imposes a limit on the current of low-velocity electrons, since too strong a current would erase the charge image too completely.

Owing to these effects it is most unlikely that the flooding method will produce a sensitivity equal to that of an image iconoscope operating ideally to give a signal current roughly 1.3 (δ_{max}—1) times the photo-current.

[8]) R. Theile, Arch. elektr. Übertragung **7**, 333, 1953.

Dissipation of the charge by conduction

In essence, the above two methods of accelerating the drop in potential of the target elements both consist in supplying negative charge to the surface of the target from an outside source, that is, either from electrons of the scanning beam, or from others emitted by an auxiliary photo-cathode. Let us now consider another method, i.e. supplying negative charge *through the target*, or, in other words, *dissipating* positive charge energy through the target to the signal plate.

This idea was suggested in Germany as long ago as 1938, as a means of increasing the sensitivity of the ordinary iconoscope. It was employed in what is known as the "Halbleiter-Ikonoskop" [9]). Here, maximum sensitivity is obtained at a certain value of the scanning current, but the target elements are stabilized at a potential remaining appreciably lower than that of the collector. Owing to this stabilization, for reasons which cannot be discussed here, the images of moving objects in the scene become vague. Hence this method was not then adopted for ordinary television.

In the Philips Laboratories, the principle of charge-dissipation through the target has now been applied to the image iconoscope. These experiments led to the development of the "Scenioscope," which will now be described more fully.

The "Scenioscope"

The essential difference between image iconoscope 5854 and the "Scenioscope" lies in the target. A glass plate (*fig. 7*) having a certain conductivity is substituted for the insulating mica plate employed in the image iconoscope. The back of it is covered with a layer of metal, acting as a signal plate and assuming a negative potential with respect to the collector. As in the image iconoscope, the scanning beam periodically stabilizes the surface elements of the target at a potential slightly higher than that of the collector. The potential of a particular element drops in the interval between successive scannings, partly owing ito the interception of redistributon electrons, but mainly because of the leakage current through the target. The dominance of the leakage current as compared with the redistribution is conducive to the elimination of spurious signals.

The leakage current can be varied by varying the D.C. voltage on the signal plate. The size of this current governs the maximum white level of the tube output signal, since the photo-current at the

[9]) G. Krawinkel, W. Kronjäger and H. Salow, Über einen speichernden Bildfänger mit halbleitendem Dielektrikum, Z. techn. Phys. **19**, 63-73, 1938.

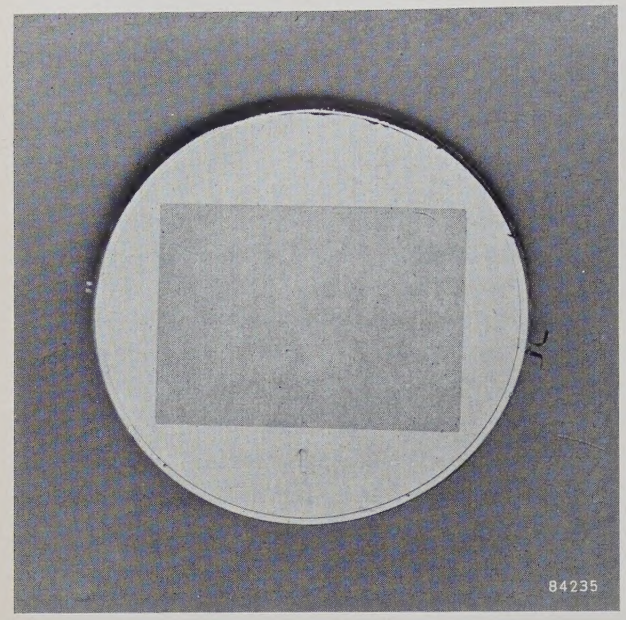

Fig. 7. The target of the "Scenioscope" is a thin plate of slightly conductive glass, from 50 to 70 μ thick, on a metal ring. The size of the rectangular area scanned is 45 × 60 mm. The signal plate is a layer of metal on the back of the target.

"brightest" points can at most only compensate for the charge which is dissipated. In theory the maximum quantity of charge that a target element can collect is equal to the charge increment supplied during scanning to non-illuminated elements; increasing the leakage current, by giving the signal plate a more negative bias, therefore enables a heavier picture-charge to be stored.

Considered superficially, it may well seem odd to make the target conductive, since this enables a certain amount of the charge pattern to leak away. As will be explained below, however, careful design reduces the loss of sensitivity owing to this leakage to a mere fraction of the gain resulting from the fact that the accelerated potential drop enables the photo-electrons to contribute sooner to the build-up of the potential image.

Before discussing the sensitivity of the "Scenioscope", we shall consider the following points: the elimination of spurious signals, the measures taken to overcome certain difficulties (amongst other things, the charge pattern leakage already referred to) and the requirements imposed on the glass target.

The avoidance of spurious signals

As the potential V of a target element drops in the interval between successive scannings, the number of redistribution electrons trapped by the element decreases, until finally the potential is affected only by the leakage current (*fig. 8*). With a negative signal plate, this current forces V below the cut-off limit V_0 for secondary electrons proceeding to the target element. Accordingly, the leakage current does not depend upon the position of the element on the target plate and, unlike the redistribution effect, does not produce spurious signals. To avoid such signals, then, the effect of redistribution should be kept as small as possible compared with that of leakage current (here is a fundamental difference in operating conditions between the image iconoscope and the "Scenioscope": in the one the redistribution effect is essential, whereas in the other it is merely incidental). Since the redistribution current to a particular target element decreases sharply with the potential of the element, the need is to force the potential below the value at which redistribution still occurs (that is, roughly between V_{coll} and V_0, fig. 8) as quickly as possible. Apart from increasing the sensitivity, then, a sharp drop in potential also tends to suppress spurious signals.

The potential drop can be accelerated in two ways, viz. by increasing the leakage current, or by reducing the capacitance of the particular element with respect to the signal plate. The permissible

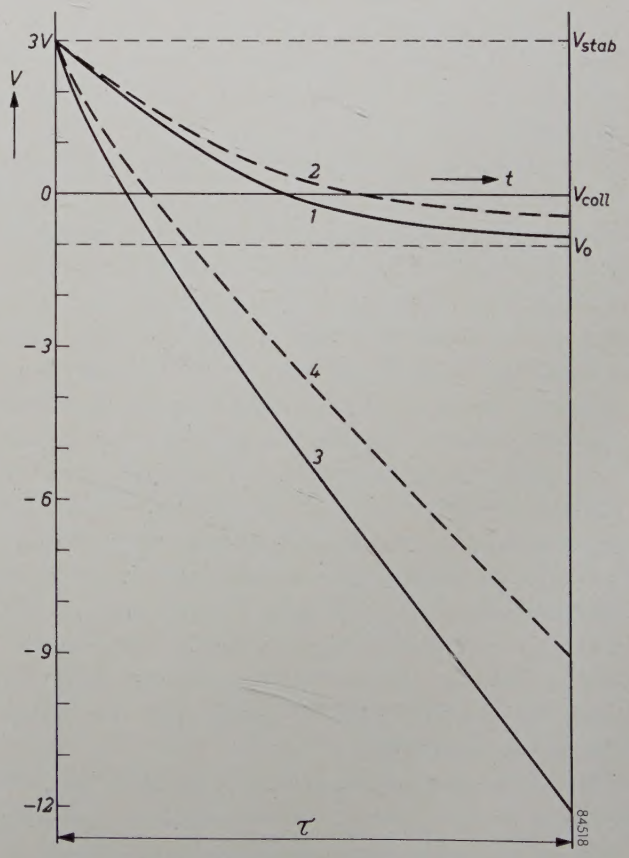

Fig. 8. *1* and *2* are $V = f(t)$ curves, as shown in fig. 3*b*, for the image iconoscope. *3* and *4* refer to the "Scenioscope" (slightly conductive target, signal plate potential negative), *3* for a non-illuminated, and *4* for a faintly illuminated photo-cathode.

increase in leakage current is limited owing to the fact that it produces undue electrolysis in the glass, thus shortening the life of the tube. With a heavy leakage current, moreover, any local variation in the thickness of the target plate, however slight, would cause a local difference in this current, proportional, of course, to the overall leakage, thus producing spurious signals.

Similarly the reduction of capacitance by increasing the thickness of the target plate is limited by the high resolving power required (see below) and, as will be explained later, the requirement as to shape imposed on the tube characteristic.

Leakage of the charge pattern

Theoretical considerations have shown[10]) the extent to which the charge pattern is affected by the conductivity of the glass and the thickness of the target plate. The conductivity of the glass affects the output signal in two ways: by conduction perpendicular to the surface of the target (i.e. in the axial direction of the camera tube) and by transverse conduction, parallel to the surface. Despite the fact that it increases the sensitivity, then, this conductivity must not be too high.

Consider first the axial conduction. This dissipates part of the impressed picture-charge before the next scanning enables it to contribute to the output signal. The amount of charge thus dissipated depends upon the relaxation time (R_0C_0) of the target plate (R_0 being the resistance and C_0 the capacitance, both per unit area, between the front of the target and the signal plate). *Fig. 9* shows the

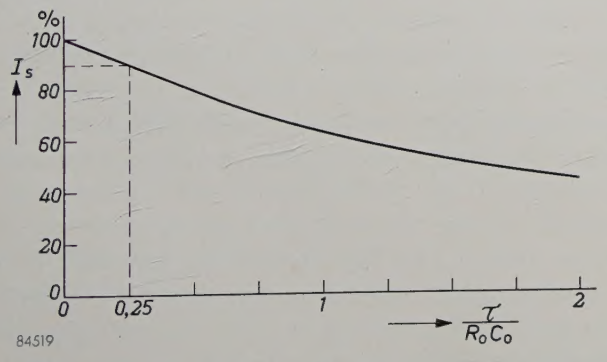

Fig. 9. Signal current (I_s; on relative scale), plotted as a function of τ/R_0C_0. The values of R_0 and C_0 are chosen so as to give an I_s equal to 90% of the maximum value ($\tau/R_0C_0 = 0.25$)

signal on a relative scale plotted against τ/R_0C_0, τ being the frame period ($^1/_{25}$ second in European television systems).

Owing to this effect, a certain loss of sensitivity must be accepted and, as will be seen from fig. 9, to limit this loss to 10% we must ensure that τ/R_0C_0 does not exceed 0.25. Now, for τ/R_0C_0 we may write: $\tau/\varepsilon_0\varepsilon_r\varrho$, where ε_0 is the dielectric constant of free space, ε_r the relative dielectric constant of the glass and ϱ the volume resistivity of the glass. Substituting $\tau = 1/25$ second, $\varepsilon_0 = 8.86 \times 10^{-12}$ F/m and $\varepsilon_r = 8$, we find that for $\tau/R_0C_0 = 0.25$, the volume resistivity ϱ must be $> 0.23 \times 10^{12}$ ohm cm to ensure that the loss of sensitivity owing to leakage will not exceed 10%.

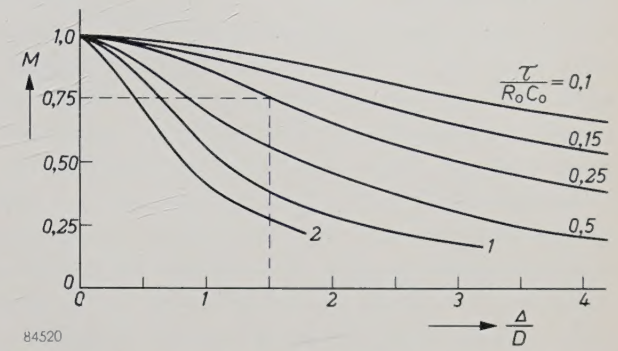

Fig. 10. Relative modulation depth M of the potential pattern on the target, plotted against Δ/D (Δ = thickness of target, D = width of bands in a picture comprising black and white bands), for various values of τ/R_0C_0. With $\tau/R_0C_0 = 0.25$, Δ/D must not exceed roughly 1.5 if the modulation depth is to be maintained at a reasonable value.

Secondly, consider the transverse conduction between a given picture element and adjacent elements with a relatively lower illumination level. Such leakage causes a loss of definition, all the more serious, of course, for the smallest details of the picture, where it also gives rise to loss of contrast. For a picture comprising light and dark bands, for example, the result of transverse conduction will be that the narrower the bands, the smaller the percentage modulation of the charge pattern (that is, the weaker the output signal).

To explain this effect more fully, we shall define a certain relative modulation depth M as the ratio of the signal associated with a band of given width D to that with a picture containing only one black-to-white transition. We then calculate M as a function of Δ/D (Δ being the thickness of the target) for different values of τ/R_0C_0. The results of this calculation [10]) are shown in *fig. 10*, from which it is seen that the thinner the glass (Δ) and the higher its volume resistivity (ϱ), the higher the resolving power.

What, then, are the most suitable values of ϱ and Δ? Fig. 10 requires that a high value of ϱ is chosen with a view to the resolving power, and fig. 9 requires a minimum value 0.23×10^{12}

[10]) P. Schagen, Limiting resolution due to charge leakage in the "Scenioscope", a new television camera tube, Philips Res. Rep. **10**, 231-238, 1955 (No. 3).

ohm cm in order to limit the loss of sensitivity. Accordingly, 0.3×10^{12} ohm cm is taken as the minimum, and 10^{12} ohm cm as the maximum limit; a higher value of ϱ would give rise to undue interference from edge flare, an effect which will be described later.

The glass used has a negative temperature coefficient of resistance. The above-mentioned limits of ϱ hold good for temperatures between 35 and 45 °C; hence the working temperature of the camera must be maintained within this range. At room temperature, ϱ should be between roughly 10^{12} and 3×10^{12} ohm cm.

As regards the thickness (Δ) of the glass, it is seen from fig. 10 that when $\tau/R_0C_0 = 0.25$, the ratio Δ/D must not be very much higher than 1.5, in order to maintain a reasonably large modulation depth (say, $M = 0.75$). The diameter of the smallest resolvable detail in the image equals that of one picture element; with the "Scenioscope" in a 625-line system, it is roughly 75 μ. Hence we see that, even for the smallest practical value of D, that is d (= 75 μ), a glass thickness between 50 and 70 μ, as here employed, is consistent with a Δ/D ratio well below the prescribed limit (1.5). Accordingly, we may expect the resolving power to be high; in fact, experiments have shown that with ϱ between 0.3×10^{12} and 10^{12} ohm cm, it is very nearly equal to that of image iconoscope 5854. *Fig. 11* shows the measured modulation depth at the centre of the image plotted against the number of lines per frame.

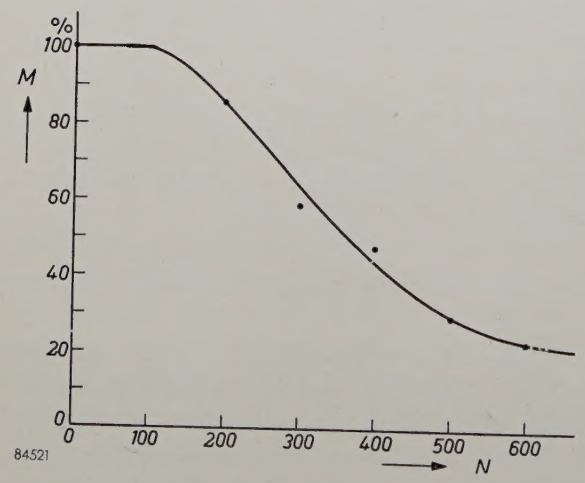

Fig. 11. Relative modulation depth M in the output signal of the "Scenioscope" for the centre of the picture, plotted against the number of lines per frame N.

Edge flare

Although the overall diameter of the circular target is roughly 80 mm, the area actually scanned is a rectangle only 45 by 60 mm (fig. 7). Experiments have shown that it is best to bound this area with a conductive frame whose potential can be taken slightly lower than that of the collector. Without this frame, the part of the target not scanned assumes the potential of the signal plate, owing to the conductivity of the glass. This potential being very much lower than that of the area scanned the elements at the edge of the image are prevented from producing their full secondary emission and therefore assume a relatively low equilibrium potential. The elements at the edge thus acquire a lower potential relative to the signal plate than the centre ones, and hence a smaller leakage current. The charge increment supplied during scanning is therefore smaller at the edge than in the middle of the image, that is, white edges appear in the received picture (edge flare). It is evident that the conductive frame will suppress this effect provided that it is given a suitable potential.

If the limit of scanning does not coincide exactly with this frame, the outer picture elements will continue to be affected to some extent by the adjoining, un-scanned target elements. Hence the potential of the signal plate must not be taken too low; as already explained, this also imposes a maximum limit on the volume resistivity of the glass.

If the potential of the signal plate with respect to the collector is, say, —50 V, and the scanning area is properly covered by the beam, the screening frame will keep the picture almost entirely free from perceptible edge flare. In practice it is found that a leakage current of 0.5 μA through the target gives very good results. With a volume resistivity of, say, 0.5×10^{12} ohm cm, the signal plate bias required to produce this current is roughly —50 V. For a target of the prescribed thickness, viz. 50-70 μ, and a leakage current of 0.5 μA, the potential-variations of the non-"illuminated" target elements are in the region of 7 V. Under the above-mentioned conditions, the redistribution effect, noticeable mainly during the traversing of the first two or three volts below the equilibrium potential, is so small that the received picture contains virtually no perceptible spurious signals. Accordingly, the sensitivity limitation when the light-level is reduced is imposed solely by noise.

The characteristics of the "Scenioscope"

With adequate leakage current, the potential of target elements having a low illumination-level drops quickly enough to enable the coefficient δ_{eff} of the photo-current to reach its maximum very soon after a scanning. Initially, then, the signal current (I_s) versus photo-current (I_{ph}) characteris-

tic of the tube is a straight line (gamma = 1). With increasing photo-current, however, the potential drop of the target elements in the intervals between scanning becomes smaller and smaller; hence the δ_{eff} of the photo-electrons takes longer and longer to reach its maximum, and finally falls short of it. The characteristic therefore exhibits a gradual saturation. The shape of the part of the characteristic where this saturation begins is governed mainly by the capacitance of the target. The lower this capacitance (that is, the thicker the target), the higher the photo-current at which saturation begins (the leakage current being constant); the characteristic may then show quite a sharp bend. With a higher capacitance, the drop in the potential of the target elements will be smaller, and a more gradual saturation will begin at a relatively lower photo-current; it reduces the sensitivity of the tube slightly (smaller signal current for the same photo-current) but at the same time offers two advantages.

Firstly, the gamma is then smaller than unity over a relatively larger part of the characteristic, as in the image iconoscope. This largely compensates for the opposite curvature of the picture tube characteristic (luminance versus control voltage), thus enabling gamma correction to be dispensed with.

Secondly, the more gradual saturation means that the maximum signal is obtained only at a far higher photo-current, enabling the tube to reproduce a higher ratio of scene contrast.

The leakage current through the target governs the photo-current level at which the characteristic begins to bend. It is found that with the prescribed leakage current of 0.5 μA, a glass-thickness of 50-70 μ produces a very suitably shaped characteristic. *Fig. 12* shows characteristics of the "Scenioscope" for three values of the leakage current, and, for comparison, the characteristic of image iconoscope 5854.

The sensitivity of the "Scenioscope"

The higher sensitivity of the "Scenioscope" as compared with the image iconoscope is attributable mainly to the conductivity of the glass target, which accelerates the potential drop of the target elements in the intervals between scannings and thus brings the ratio I_s/I_{ph} closer to the theoretical ideal $1.3(\delta_{max}-1)$.

However, a not inconsiderable part of the improvement is due to an increase in the secondary emission factor δ_{max}. In the image iconoscope 5854, as explained in article [1]), $\delta_{max} \approx 4$. By virtue of certain special features of design, the δ_{max} of the "Scenioscope" is raised to between 8 and 10. It is seen from the characteristics shown in fig. 12, that the sensitivity of the "Scenioscope" is not very far below the maximum value theoretically attainable with such a system at the above value of δ_{max}: at the start of the characteristic, I_s/I_{ph} is roughly 7, whereas a value in the region of 10 is theoretically possible.

The lowest light-level at which good picture quality is obtained is limited by the noise level, not, as in the image iconoscope, by the spurious signals. The compensating signals which have to be applied to the amplifier of an image iconoscope to suppres spurious signals, are therefore not necessary for the "Scenioscope".

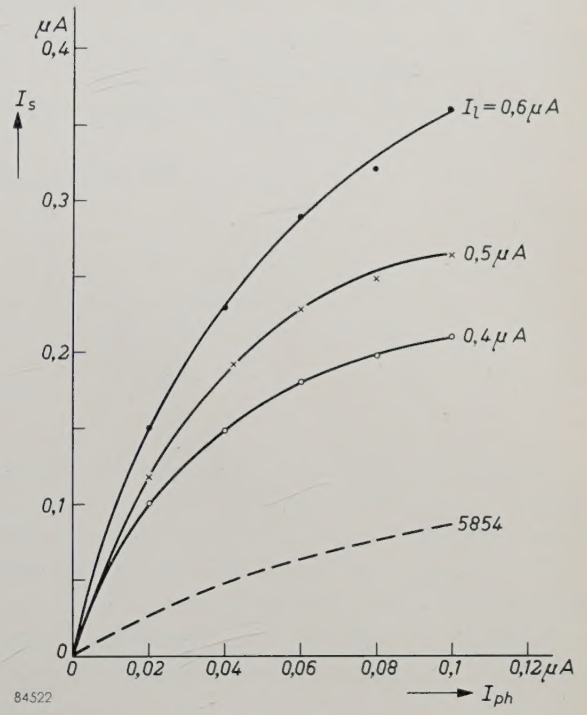

Fig. 12. Full curves: I_s as a function of I_{ph} for the "Scenioscope" for various values of the leakage current I_l through the glass target (I_l measured in darkness). Broken curve: $I_s = f(I_{ph})$ for image iconoscope 5854 (from fig. 4).

With a properly matched amplifier producing very little noise, acceptable pictures are obtained with only 100 lux of illumination on the scene, and under practical operating conditions roughly 300 lux is enough to ensure a virtually noise-free picture (lens aperture $f:2$).

It will be evident that, apart from the difference in sensitivity, the characteristics of the "Scenioscope" and the image iconoscope are very much the same; the photo-cathodes, electron-optical image-forming systems and electron guns of the two tubes are identical. The "Scenioscope" therefore also

admits the facility of continuous variation of the field of view by electrical means (see the article referred to in note [2]).

Summary. Experiments with the image iconoscope have shown that the sensitivity of such a tube can be increased if the potential drop of the target elements in the intervals between scannings can be accelerated. In certain camera tubes now on the market, this is accomplished by "flooding" the target with low-velocity electrons from an auxiliary photo-cathode provided with variable illumination. Another method, simpler and more effective, is employed in a new tube developed by Philips. In this tube, the "Scenioscope", a target of glass having a certain conductivity is employed instead of one made of non-conductive mica. The volume resistivity of the glass and the thickness of the target are considered. The effect of redistribution, a source of spurious signals, is minimized by increasing the leakage current through the glass. Hence the minimum limit of illumination is imposed not by interference from spurious signals, but merely by noise. Whereas redistribution is essential in the image iconoscope, it is merely incidental in the tube considered here. The signal current versus photocurrent characteristic of the "Scenioscope" has a curvature opposite to that of the luminance versus control voltage characteristic of a picture tube, thus enabling gamma correction to be dispensed with.

The gain in sensitivity as compared with the image iconoscope is attributable partly to the conductivity, and partly to the relatively higher secondary emission factor of the target. A picture of acceptable quality is obtained with only 100 lux of illumination on the scene, and in practice 300 lux is enough to ensure a virtually noise-free picture (lens aperture $f:2$).

THE "TL"F LAMP, A TUBULAR FLUORESCENT LAMP WITH A DIRECTIONAL LIGHT DISTRIBUTION

by J. J. BALDER and M. H. A. van de WEIJER. 621.327.534.15

This article introduces a newly developed type of "TL" lamp, which, especially in dusty locations, provides a considerable improvement in light output.

Normal tubular fluorescent lamps ("TL" lamps) display a uniform brightness over the whole of their cylindrical surface (if we discount the short lengths at the tube extremities, where end-effects appear). The light distribution curve of such a lamp in a plane perpendicular to the tube axis is thus a circle (*fig. 1a*). For many applications, however, it is desirable that the light radiated should mainly be concentrated within a given solid angle. It is, for example, very often desired that the light be directed for the most part onto the working plane. This can be achieved by use of a suitable lighting fitting. With such a reflecting fitting, for example, a light distribution curve like that shown in fig. 1*b* can be obtained.

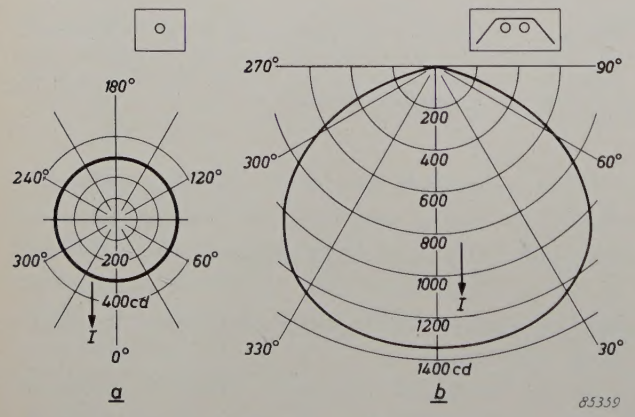

Fig. 1. *a*) Light distribution curve (polar diagram of the luminous intensity in candelas as a function of the direction) in a plane perpendicular to the axis of a normal 40 W "TL" lamp. The curve is a circle.
b) The same for a trough fitting (see inset) with two normal 40 W "TL" lamps. The reflector directs the light downwards.

Influence of dust and dirt

The diagrams of fig. 1 hold for a lamp, or lamps and fittings, which are clean. These diagrams are unfavourably influenced, however, by the inevitable fouling of lamp and fitting occurring in practice due to dust etc. On the lamp itself, in the course of time, a layer of dust settles on the upper surface. This occurs, though to a lesser extent, even when a reflector is placed above the lamp. The influence of an even layer of dust with a transmission factor $\tau_v = 0.5$ coated on the upper half of a normal "TL" lamp can be seen in *fig. 2a* and *b*. Even in places which are not excessively dusty, τ_v reaches the value of 0.5 within a few months of the insertion

or cleaning of the lamps. In very dirty places it is even found that the dust layer becomes practically opaque. The light distribution curve of such a dirty lamp ($\tau_v = 0$) is also shown in fig. 2*a*.

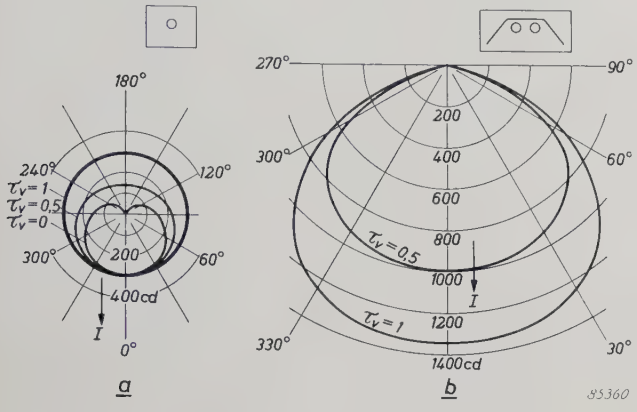

Fig. 2. *a*) Light distribution curves for normal "TL" lamps coated on the upper surface with a uniform layer of dirt, having a transmission factor τ_v. The curve for $\tau_v = 1$ (clean lamp) is identical to that in fig. 1*a*.
b) Light distribution curves for a two-lamp trough fitting holding normal "TL" lamps evenly coated with dirt on the upper surface. The curve for $\tau_v = 1$ is identical to that in fig. 1*b*.

"TL" lamps with directional light distribution ("TL"F lamps)

In the case of the newly developed "TL"F lamp, which forms the subject of this article (F is the type-indication), fouling has much less influence than with the usual lamp types. In the new lamp the light distribution curve is no longer circular, the light being mainly directed to one side (*fig. 3a*). Its is thus possible to mount the lamp in such a way that only a relatively small proportion of the light is radiated upwards. A layer of dust on the top of the lamp then has only a very slight influence on the total luminous flux radiated.

The directional effect can be obtained by making the fluorescent powder layer, with which the inside wall of the tube is coated, thicker than normal over a portion (about 230°) of the tube circumference. The reflection factor of a powder layer increases with the thickness of the layer, so that we obtain in this way a (diffuse) reflector inside the tube. In the lamp described in the present article the increase in reflection factor is obtained by incorporating, between the fluorescent powder layer and the glass wall, a separate layer of powder which does not fluoresce but which possesses very good reflection characteristics. That part of the lamp where fluorescent powder alone is applied forms as it were a slot through which the greater portion of the luminous flux emerges (*figs. 4* and 5). This part of the radiating surface will be referred to below as the "slot".

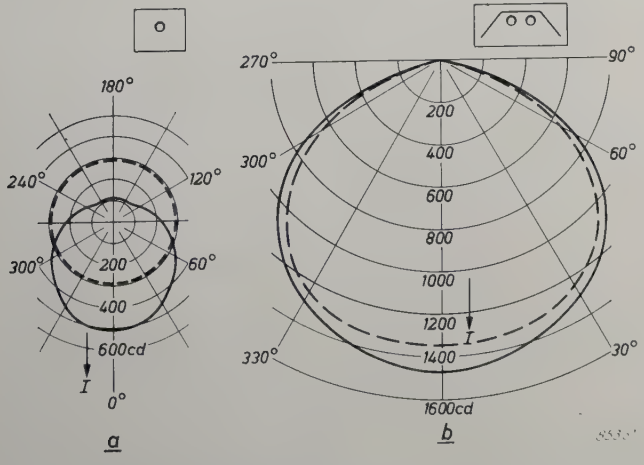

Fig. 3. Light distribution curve of the new 40 W "TL"F lamp with directional radiating characteristics (*a*) and for two of these lamps in a trough fitting (*b*). For comparison purposes the corresponding curves for the normal lamp, taken from fig. 1*a* and *b*, are indicated with broken lines.

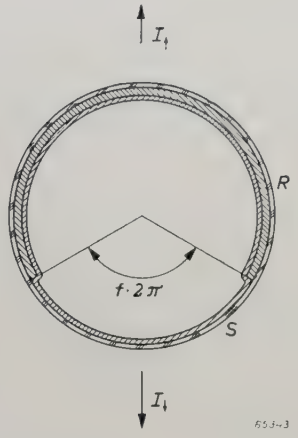

Fig. 4. Schematic cross-section of a "TL"F lamp. The portion *S*, subtending an angle $2\pi f$, is coated only with a normal fluorescent powder layer. This portion forms the so-called slot. Over the rest of the circumference, i.e. the portion *R*, a layer of powder of good reflection properties is applied between the fluorescent powder and the glass wall. The portion *R* has thus a higher reflection factor, and also a greater absorption factor than the portion *S*. $I\downarrow$ represents the luminous intensity vertically downwards, and $I\uparrow$ the luminous intensity vertically upwards.

Fig. 6 gives light distribution curves for the new lamp, compared with those of a normal lamp, in both clean and dirty conditions.

We shall now firstly consider how the radiated luminous flux in a normal "TL" lamp is produced. It will then be possible to give the results of calculations for the "TL"F lamp without discussing them in great detail. Secondly, we shall give the results of the comparative measurements on normal "TL" lamps and "TL"F lamps, in the form of graphs and in a table.

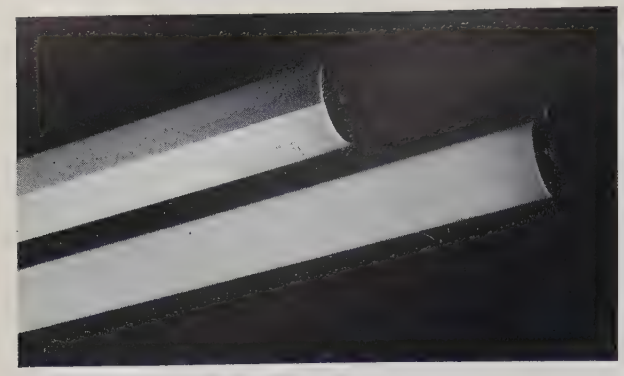

a

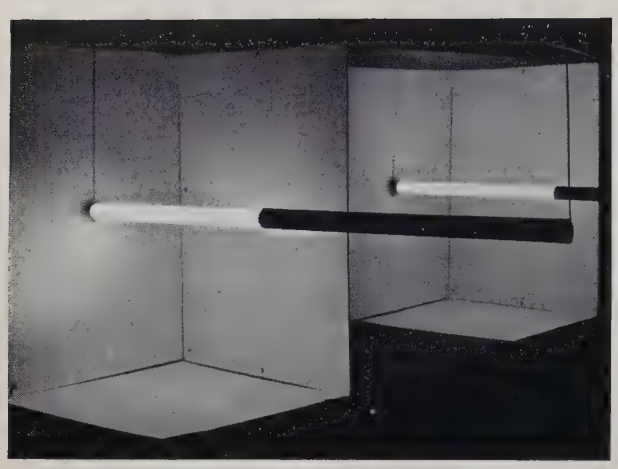

b

Fig. 5. *a*) "TL" lamps in operation; a normal lamp and a lamp with directional distribution ("TL"F lamp, in the foreground). In the "TL"F lamp the brightness is low where the reflecting layer is present between the fluorescent powder layer and the glass wall. The light is mainly emitted through the bright slot (angular width about 130°).
b) Illumination with a "TL"F lamp (foreground), compared with illumination with a normal "TL" lamp (background), in both cases without a fitting. With the "TL"F lamp the lower portion of the cabinet is more strongly illuminated, and the upper portion less so, than is the case with the normal lamp.

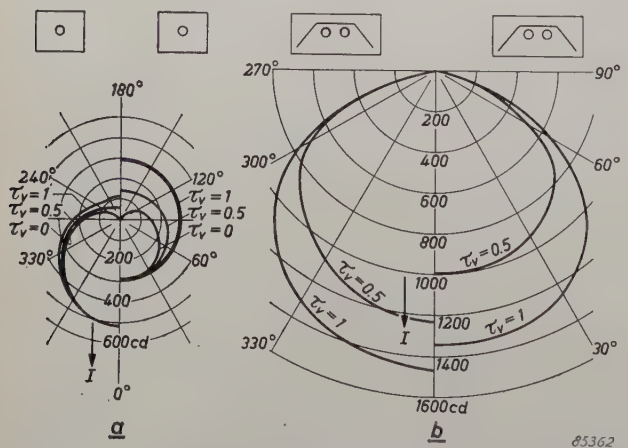

Fig. 6. *a*) The light distribution curves for "TL"F lamps with dirt layers on the upper half having the same values of τ_v as in fig. 2*a* are shown on the left. The slot is directed downwards. For comparison purposes, the curves of fig. 2*a* for the normal lamp are reproduced on the right.
b) The same for a two-lamp trough fitting with dirty "TL"F lamps. The curves on the right of the figure are for normal "TL" lamps as already given in fig. 2*b*.

Light production of a normal "TL" lamp

When light falls on a glass surface coated with a uniform layer of powder, a fraction τ is transmitted, a fraction a absorbed, and a fraction ϱ reflected. τ, a and ϱ are termed respectively the transmission, absorption and reflection factors. Clearly, $\tau + a + \varrho = 1$. We will consider only a powder layer for which both the transmitted and the reflected light are diffuse.

The powder coating on the inside wall of a "TL" lamp fluoresces under the influence of the ultraviolet radiation produced by a gas discharge maintained inside the tube. Due to the high absorption factor of the powder for the ultraviolet radiation, the visible fluorescent light is excited in a thin layer on the surface of the powder. If we assume that this surface layer is infinitely thin — for our purpose a sufficiently close approximation to the truth — then of the total primarily excited luminous flux Φ_p, a half is sent out in the direction through the powder layer. This half of the flux can be regarded as if it fell on the powder layer from inside the tube. The other half is radiated from the surface of the powder towards the inside of the tube, but must, since the surface is in itself closed (a cylinder), nevertheless meet the powder layer again somewhere else. (The tube is assumed long compared with its diameter so that the loss of light at the extremities of the tube may be neglected.) For the purposes of calculation, therefore it may be taken that all the primary luminous flux Φ_p falls on the inside wall of the tube.

Of this incident luminous flux, $\varrho\Phi_p$ will be reflected and thrown back onto the wall of the tube. This time $\varrho^2\,\Phi_p$ will be reflected, and so on. The total luminous flux Φ_i falling on the tube wall is thus:

$$\Phi_i = \Phi_p\,(1 + \varrho + \varrho^2 + \ldots) = \frac{\Phi_p}{1-\varrho}. \quad . \quad . \quad . \quad (1)$$

The fraction τ of Φ_i is transmitted and the fraction a is absorbed. The useful luminous flux Φ emerging from the tube is thus:

$$\Phi = \tau\Phi_i = \frac{\tau}{1-\varrho}\,\Phi_p. \quad . \quad . \quad . \quad . \quad (2)$$

The absorbed luminous flux Φ_a is

$$\Phi_a = a\Phi_i = \frac{a}{1-\varrho}\,\Phi_p. \quad . \quad . \quad . \quad . \quad (3)$$

Clearly, $\Phi + \Phi_a = \Phi_p$, the primary luminous flux generated inside the tube.

A thick powder layer causes, in two ways, an increase in the absorption and thus a decrease in

the useful output of the lamp. Firstly, a itself becomes greater, since the distance to be traversed through the layer by the light increases, and, secondly, ϱ also becomes greater, resulting in an increase in Φ_i and Φ_a (One may not, of course, deduce from (2) that an increase in ϱ produces an increase in Φ, the emergent luminous flux, since an increase in ϱ is accompanied by a decrease in τ). It follows from this argument that an infinitely thin layer of powder would be the most favourable. In actual fact there is an optimum thickness of layer, since a certain thickness is needed to absorb the ultraviolet radiation and also, with very thin layers, gaps occur in the fluorescent powder as a result of the finite grain size of the powder.

Light production of the "TL"F lamp

As mentioned earlier, the "TL"F lamp is coated over a fraction f of its circumference (viz. the so-called "slot") with normal fluorescent powder only, whilst on the remainder of the circumference, a layer with good reflection characteristics is applied under the fluorescent powder layer. Quantities associated with the slot will be distinguished by the suffix S and those associated with the reflecting layer by R; values associated with a normal lamp (i.e. a lamp for which $f = 1$) will be given the suffix n.

The ratio of various characteristics of the "TL"F lamp to the corresponding values for the normal "TL" lamp, are set out in *fig.* 7 as a function of the slot width f. We shall not deal here in detail with the calculations upon which these curves are based, but confine ourselves to an explanation of the general form of the curves.

We shall begin with the values of the *luminance* B observed at the outside surface of the tube. The luminance at a given place is proportional to the emergent luminous flux per sq. cm., and thus to the internal illumination multiplied by the transmission factor τ_S or τ_R ($\tau_S > \tau_R$) at that place. If the internal illumination is everywhere uniform in the lamp, then the luminance values are proportional to the transmission factors.

If we imagine the thicker powder layer as being so narrow (f practically equal to 1) that it does not appreciably influence the internal reflections, then the internal illumination remains equal to that in a normal lamp, so that $B_S = B_n$, whilst $B_R = (\tau_R/\tau_S)B_n$.

In the other extreme case, where the thicker powder layer covers practically the whole of the circumference (f practically equal to 0), the internal illumination is almost equal to that which would occur if the slot width was actually zero. The total luminous flux falling on the internal surface is given in this case (see equation (1)) by $\Phi_p/(1-\varrho_R)$. In the normal case ($f = 1$) this was $\Phi_p/(1-\varrho_S)$, so that it has been increased by a factor $(1-\varrho_S)/(1-\varrho_R)$. ($\varrho_R$ is $> \varrho_S$). The internal illumination

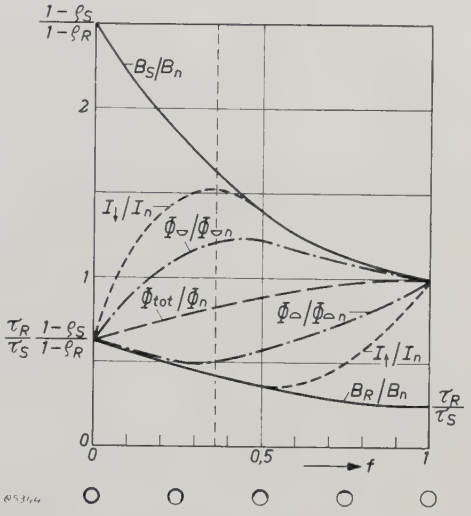

Fig. 7. Theoretical curves of various illumination quantities, as functions of the relative slot width f, all expressed as ratios with respect to the corresponding values for a normal lamp ($f = 1$, suffix n). The following values are plotted: B_S and B_R the luminance of the slot and of the remainder of the lamp surface, respectively; the luminous intensity $I_\downarrow$ vertically downwards and the luminous intensity $I_\uparrow$ vertically upwards; the luminous flux radiated into the lower hemisphere and that radiated into the upper hemisphere, $\Phi_\triangledown$ and $\Phi_\triangle$ respectively, and the total luminous flux Φ_{tot}. For the reflection, absorption and transmission factors of the slot and the remainder of the lamp surface, we have assumed, for the purpose of this example, the values $\varrho_S = 0.69$, $\alpha_S = 0.01$, $\tau_S = 0.30$ and $\varrho_R = 0.875$, $\alpha_R = 0.05$, $\tau_R = 0.075$, these being the actual values for some of the powder layers used in the experiments.

is, therefore, now also a factor $(1-\varrho_S)/(1-\varrho_R)$ greater than in the normal case. The luminance of the (infinitely narrow) slot is also increased by the same factor:

$$(B_S)_{f=0} = \frac{1-\varrho_S}{1-\varrho_R} B_n.$$

B_R is again smaller than B_S: for $f = 0$, $B_R = (\tau_R/\tau_S)B_S$, so that

$$(B_R)_{f=0} = \frac{\tau_R}{\tau_S} \frac{1-\varrho_S}{1-\varrho_R} B_n.$$

As f increases from 0 to 1, i.e. as the slot width increases, the average reflection factor gradually decreases from ϱ_R to ϱ_S and thus the total luminous flux falling on the inside of ths lamp wall correspondingly decreases from $\Phi_p/(1-\varrho_R)$ to $\Phi_p/(1-\varrho_S)$. The luminances B_S and B_R will thus decrease. Since the rotational symmetry is lost when f differs from

0 or 1, we may not expect that the internal illumination will remain independent of the position on the circumference of the lamp. The internal illumination will not even remain constant within the arc covered by S or by R, so that this will neither be the case for the luminances B_S and B_R. It proves, however, in practice, from both calculations and measurements, that the variations in luminance within the portion S and within the portion R are only small, so that by approximation one can nevertheless speak of "the" luminance B_S and "the" luminance B_R. These luminances, which are actually averages over the surfaces to which they refer, both decrease gradually as the slot width is increased, according to the curves when shown in fig. 7.

We will now consider the *luminous intensities* $I_\downarrow$ and $I_\uparrow$, i.e., the luminous intensity in the vertically downward direction and that in the vertically upward direction (with the lamp positioned as in fig. 4). As long as $1 \geqq f \geqq 0.5$, the whole of that half of the lamp visible from below has the luminance B_S and thus $I_\downarrow$ is proportional to B_S, i.e. the curve for $I_\downarrow/I_n$ coincides with that for B_S/B_n. As soon as f becomes smaller than 0.5, the outer edges of the surface visible from below acquire the much lower luminance B_R. This effect has the tendency to cause $I_\downarrow$ to decrease. Initially, the increase of the luminances B_S and B_R retains the upper hand and the curve for $I_\downarrow/I_n$ continues to rise, although less steeply than that for B_S/B_n. Gradually, however, the decrease in the area of the bright slot gains in effect; the luminous intensity vertically downwards reaches a maximum and then decreases until, for $f = 0$, the value

$$(I_\downarrow)_{f=0} = \frac{\tau_R}{\tau_S} \cdot \frac{1-\varrho_S}{1-\varrho_R} I_n$$

is reached. As will be seen from fig. 7, $I_\downarrow$ reaches its maximum value at a slot width of about 130° ($f \approx 0.36$), which is used in practice.

For $I_\uparrow$, the luminous intensity in the direction vertically upwards, an analogous reasoning applies.

The total *luminous flux* Φ_{tot} decreases as the slot is made narrower. That this must be the case can most easily be seen by remembering that the average reflection factor and the average absorption factor of the powder layer both become greater, two effects which favour an increase in absorption (see formula (3)). The ratio of the total luminous flux between the extreme cases of zero slot width and a normal lamp ($f = 0$ and $f = 1$ respectively), is of course the same as that of the luminances. The curve for Φ_{tot}/Φ_n thus commences for $f = 0$ at the same point as the curve for B_R/B_n.

Two further quantities of importance are, finally, the luminous fluxes emitted in the lower and in the upper hemispheres, indicated by $\Phi_\cup$ and $\Phi_\cap$, which are also shown in fig. 7.

For uniform lamp luminance, as obtained with $f = 0$ and $f = 1$, $\Phi_\cup$ and $\Phi_\cap$ are of course mutually equal and proportional to the luminance. For this reason the starting points ($f = 0$) of the curves for $\Phi_\cup/\Phi_{\cup n}$ and $\Phi_\cap/\Phi_{\cap n}$ coincide with the starting-point of the curve for B_R/B_n, and their terminal points ($f = 1$) with the end-point of the curve for B_S/B_n. The curve for $\Phi_\cup/\Phi_{\cup n}$ shows, in the neighbourhood of $f = 1$, a tendency to follow the curve for B_S/B_n. Since also the upper part of the lamp radiates some light into the lower hemisphere, the darker portion R of the lamp begins to exert an influence on $\Phi_\cup$ as soon as f differs from 1. Hence $\Phi_\cup/\Phi_{\cup n}$ is immediately less than B_S/B_n. The maximum can be explained in the same way as that in the curve of $I_\downarrow/I_n$. The curve of $\Phi_\cap/\Phi_{\cap n}$ can be explained qualitatively in a similar manner.

Fig. 8 gives the light distribution curves of a series of experimental lamps in which the influence of the slot width was investigated. It can be seen, for example, how the luminous intensity in a vertically downwards direction, reaches a maximum for a

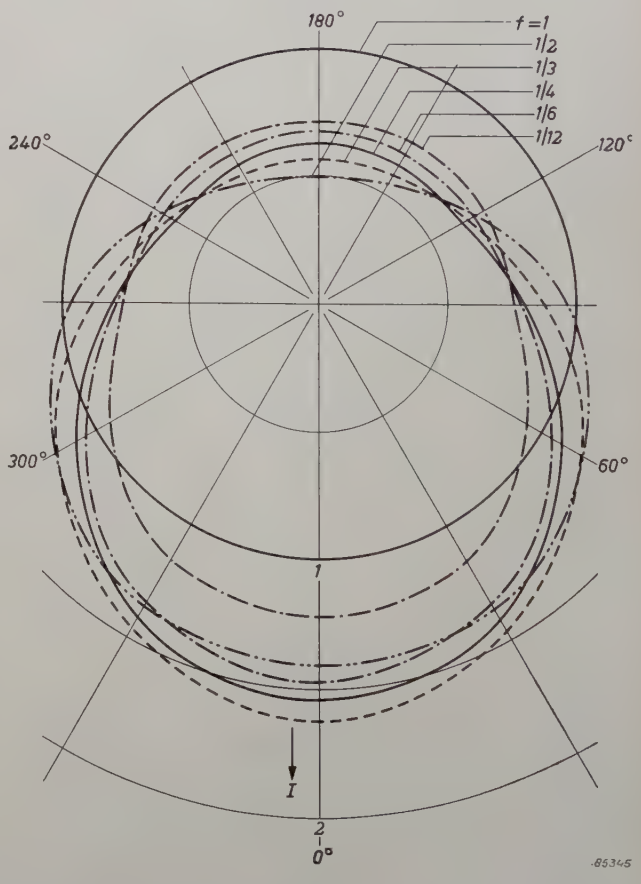

Fig. 8. Light distribution curves for a series of experimental lamps with increasing slot width, f. In these preliminary experiments the optimum properties of the powders had not yet been chosen. The luminous intensity of a normal lamp ($f = 1$) is taken as unity.

value $f < 0.5$, in agreement with the theory. No special attention was paid, in these preliminary experiments, to achieving an optimum combination of powder properties.

Comparative measurements on normal "TL" lamps and "TL" F-lamps

Lamps without fittings

A comparison of the light distribution curves of normal lamps and "TL"F lamps, in clean condition and in two degrees of dirtiness has already been given in fig. 6*a*. *Fig. 9*, which is derived from a combination of measurements and calculations, provides some further details regarding the influence

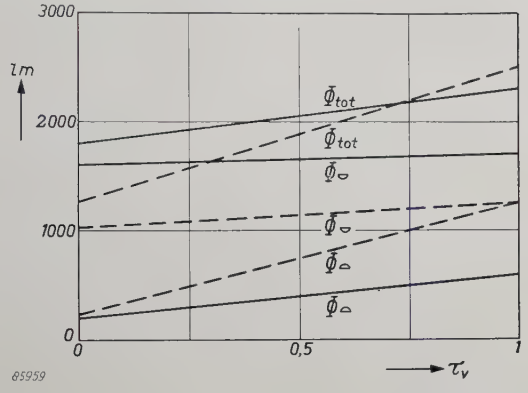

Fig. 9. Effect of a dirt layer on the upper surface on the performance of "TL"F lamps (full lines) and of normal "TL" lamps (dotted lines). The transmission factor τ_v of a uniform layer of dirt on the upper surface is plotted horizontally, whilst the total luminous flux Φ_{tot}, and the luminous flux radiated into the lower and upper hemispheres, $\Phi_{\cup}$ and $\Phi_{\cap}$ respectively, are plotted vertically.

of dirt on the two types of lamps. In this figure the total luminous flux and the luminous flux sent out into the lower and into the upper hemispheres are plotted as a function of the transmission factor τ_v of the dust layer on the upper surface of the lamps. In agreement with theory, the normal "TL" lamp delivers, in a clean condition, a somewhat greater total luminous flux than the "TL"F lamp: at zero burning-hours, normal "TL" and "TL"F lamps of 40 W rating deliver 2500 and 2300 lumens respectively. Dirt has, however, much more influence on the total luminous flux of the normal lamp than on that of the "TL"F lamp, so that even with a moderate degree of dirtiness the latter shows an advantage. All graphs and data refer to lamps at zero burning hours.

Lamps in fittings

The light distribution curves of a trough fitting with two normal "TL" lamps and with two "TL"F lamps were compared in fig. 6*b*, for both clean and dirty lamps. These curves apply for a clean *fitting*. It will be apparent that, if the reflecting surface which has to cast the light downwards becomes dirty, the use of "TL"F lamps can be advantageous. *Fig. 10a* shows for normal and for "TL"F lamps in the same fitting as in fig. 6*b*, how the effective luminous flux delivered depends on the reflection

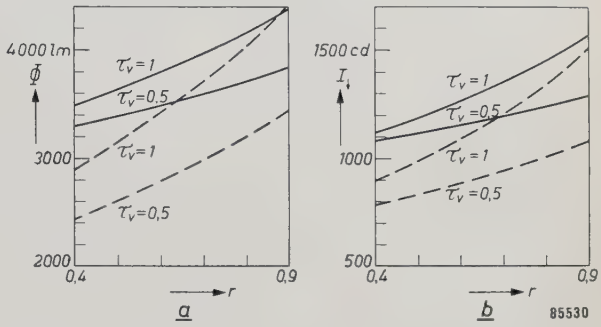

Fig. 10. *a*) Effect of the reflection factor r of the reflector of a two-lamp trough fitting on its luminous flux. The full lines refer to "TL"F lamps, the dotted lines to normal lamps. Both types of lamp were measured in a clean condition ($\tau_v = 1$) and with a layer of dirt on the upper surface ($\tau_v = 0.5$).
b) As for (*a*), but showing the effect on the luminous intensity vertically downwards, $I_\downarrow$.

factor r of the external reflector. Here, again, the results are shown for both clean lamps and lamps coated on the upper side with a dust layer for which $\tau_v = 0.5$. For a good, clean reflector the value of r is about 0.8. Even with clean lamps and a clean reflector the use of "TL"F lamps thus gives a higher luminous flux from the fitting than is obtained with

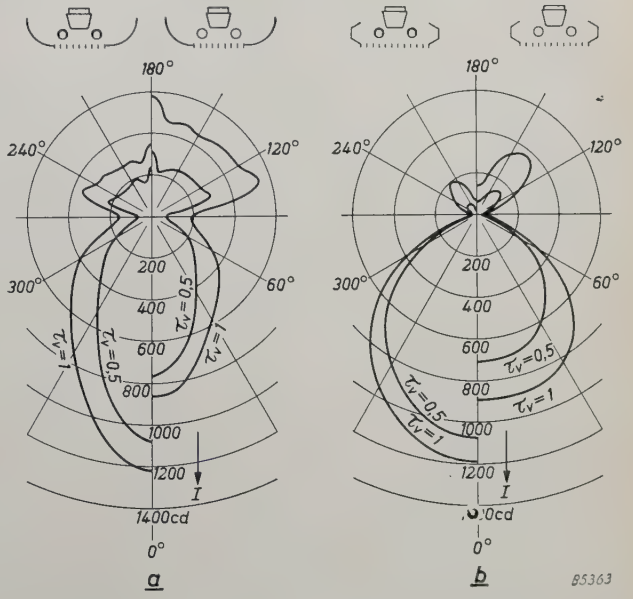

Fig. 11. *a*) Light distribution curves for a louvred fitting with translucent side-panels (see insets). The left-hand curves are for clean "TL"F lamps ($\tau_v = 1$) in a clean fitting, and for dirty "TL"F lamps ($\tau_v = 0.5$) in a correspondingly dirty fitting; the right hand curves are for normal "TL" lamps under the same conditions.
b) As for (*a*) but using a two-lamp louvred fitting with metal side-panels (see insets).

normal "TL" lamps, as can also be seen from fig. 6*b*; the effect of a layer of dirt on the lamps enhances still more the superiority of "TL"F lamps in this type of fitting. The same applies to the luminous intensity vertically downwards, as can be seen in fig. 10*b*.

In *fig. 11a* and *b* the light distribution curves for normal and for "TL"F lamps are compared for two other important types of fittings, viz. a louvred fitting with translucent sides and a louvred fitting with metal sides, both two-lamp fittings. The influence of a dirt layer is again demonstrated by plotting the curves for clean lamps in a clean fitting and for lamps covered on the upper surface with a uniform dirt layer ($\tau_v = 0.5$) in a correspondingly dirty fitting.

Illumination on the working-plane

A very important quantity in practice is the illumination on the working-plane. To compare this for "TL"F lamps and for normal "TL" lamps, 12 normal 40 W "TL" lamps in a certain type of fitting were mounted in a room 2.85 metres high with a floor area of 5×5.5 square metres. This corresponds to a lamp consumption of 17.5 watts per square metre. The illumination in a working-plane 0.75 metres above floor-level was then measured for clean lamps and for dirty lamps. Here, again, the latter had been coated on the upper surface with a uniform layer of dirt with a transmission factor $\tau_v = 0.5$. The measurements were then repeated using the same number of "TL"F lamps of the same wattage. The tests were carried out successively with various types of fittings and with lamps mounted directly on the ceiling. When mounted in fittings the lamps hung 0.35 metre below the ceiling; the distance from lamps to working-plane was thus 1.75 metres. Using ceiling-mounted lamps this distance was 2 metres. The reflection factor of the ceiling was 0.73 and that of the side walls 0.43. For ceiling-mounted lamps, the measurements were repeated with a ceiling reflection-factor of 0.55. In this latter case, as was to be expected, "TL"F lamps, in the clean condition, proved to be somewhat more advantageous than was the case with the higher ceiling-reflection factor.

A number of the measurements with dirty lamps were made with correspondingly dirty fittings. The results are presented in *Table I*.

General observations

The insensitivity of "TL"F lamps to dirt layers results, in most practical cases, in smaller costs per lux-hour on the working-plane.

The "TL"F lamp is, as already mentioned, in effect a tubular lamp with built-in reflector. A reflecting metal-surface is not used, since a higher reflection factor can be obtained with a suitable layer of powder. The powder, moreover, in contrast to a metallic mirror, transmits a proportion of the light not reflected, so that it is more efficient than a mirror.

Table I. Illumination values in the working-plane, 0.75 m above the floor, in a room of floor-area 5×5.5 m² and height 2.85 m. Illumination by twelve 40W "TL" lamps (a consumption of 17.5 watts for each square metre of floor-area), evenly spaced over the area and in cases A, B, C and D mounted on 6 two-lamp fittings. Lamps 0.35 m below the ceiling, distance from lamps to working-plane 1.75 m. In cases E and E′ the 12 lamps were mounted directly on the ceiling. The distance from lamps to working-plane was then 2 m. In all cases the ceiling reflection-factor was 0.73 (very good white), except in case E′ where it was 0.55. The reflection factor of the walls was 0.43, except for the top 0.4 m where the walls where white with a reflection factor of 0.7. The numbers give the illumination (lux) averaged over the whole measuring surface; the numbers in brackets are the maximum values measured directly under the fittings. The indication "dirty lamp" implies that the upper half of the lamp was evenly coated with a dirt-layer having a transmission factor $\tau_v = 0.5$.

	Type of fitting	Condition of fitting	Reflection factor ceiling	With normal "TL" lamps		With "TL"F lamps	
				clean lamps	dirty lamps	clean lamps	dirty lamps
A.	Trough reflector (closed) (fig. 6b)	clean refl.	0.73	780 (850)	525 (575)	785 (860)	675 (745)
B.	Trough reflector open top	clean refl.	0.73	770 (850)	530 (580)	785 (865)	685 (765)
C.	Open louvred fitting (fig. 11a) with translucent side-panels	clean	0.73	685 (765)		700 (800)	
		dirty	0.73		415 (480)		495 (580)
D.	Louvred fitting (fig. 11b)	clean	0.73	640 (700)		675 (755)	
		dirty	0.73		380 (430)		505 (575)
E.	Mounted direct on ceiling	clean	0.73	715	540	735	685
E′.	Mounted direct on ceiling	clean	0.55	630		675	

The high luminous intensity of the "TL"F lamp in the preferred direction can also be of direct benefit in some cases. It is sometimes impossible to fit a good external reflector because of limitations of space. The "TL"F lamp then provides the obvious solution.

By the use of "TL"F lamps, furthermore, saving can often be made in the cost of fittings, without a serious loss of light. In general, however, it will not prove desirable to dispense entirely with the use of fittings when employing "TL"F lamps. This is because the luminance of the slot is so high (about 13×10^3 cd/m^2), that, although the apparent area of the slot seen from many directions is quite small, screening remains advisable to avoid objectionably high brightnesses in the field of view. Suitable screening can be provided in the usual way by the use of louvres or flaps to cut off the direct view of the lamp from end or side-on. In the case of the side-on direction, protection can also be achieved by employing refracting side-panels adjacent to the lamp which deflect the light radiated sidewards into a downwards direction and out of the direction of viewing (*fig. 12*).

When "TL"F lamps are mounted "bare" against fairly dark ceilings — a practice not often followed with normal "TL" lamps because of the resultant loss of light — account must be taken of the fact that long objects parallel to the lamps will cast multiple sharp shadows, which can be objectionable. Reflections of the high brightness of the slot in polished surfaces in the field of view must be avoided, especially if these are located in fairly dark surroundings, just as care is also advisable in this respect with normal lamps.

The luminance of the darker part of the tube is sufficiently low (about 2.5×10^3 cd/m^2) to require no screening. It is possible, for example, to illuminate vertical panels with the bright portion of vertically mounted lamps directed at the panels, and to leave the visible darker portions unscreened. This technique can, of course, also be applied in horizontal reflectors with horizontal "TL"F lamps mounted "upside down", i.e. with the gap on top. Owing to the enhanced effect of dust, however, this is only advisable with dust-free fittings, in dust-free rooms, or where frequent cleaning is feasible.

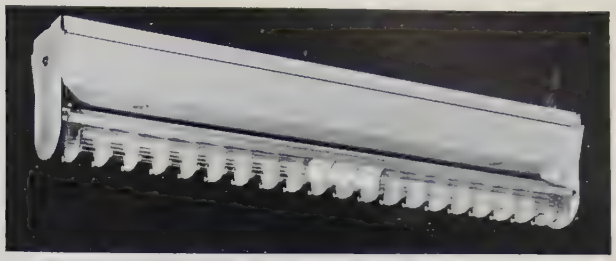

Fig. 12. Method of reducing the high brightness of the gap of a "TL"F lamp by means of refracting side-panels. The light radiated sidewards is refracted downwards. In the photograph (*a*) a portion of a side-panel in the centre has been removed. It can be seen that the brightness is much greater there than elsewhere. The principle is illustrated in the diagram (*b*).

Summary. By introducing a powder layer of good reflecting properties over a portion of the circumference of a "TL" lamp, between the fluorescent powder and the glass wall, the lamp is provided, as it were, with an internal reflector. In this way the light is radiated mainly in a preferred direction. This offers advantages when the lamps are mounted with the internal reflector at the top: deposition of dust on the upper surface then has a much smaller influence on the luminous output than is the case with normal lamps. The results of a theoretical investigation into the effect of an internal reflector of this type on various quantities of interest in illuminating engineering are discussed. On varying the angle taken up by the reflector, a maximum luminous intensity in the preferred direction occurs when this angle is approximately 230°. It is shown from the results of measurements, that even with a slight degree of dirtiness of the top part of the lamp, and in some cases even with clean lamps, the new type provides considerably better lighting than the normal type.

X-RAY INTENSITY MEASUREMENTS WITH COUNTER TUBES

by W. PARRISH *)

548.734:621.387.4:621.374.32

The use of counter tubes, which nowadays play such an important part in research, forms the basis of the method of X-ray diffraction analysis known as diffractometry. The essential advantage of this method is the relative ease with which radiation intensity measurements, for example in quantitative chemical analysis, are performed. Nevertheless, quantitative radiation intensity measurements with counter tubes have some peculiar problems, even if the radiation is nearly monochromatic as in the case of X-ray powder diffraction analysis. These problems are discussed in the present article with special reference to the various procedures of intensity measurement possible with the "Norelco" diffractometer.

Introduction

In the well known Debye-Scherrer method of X-ray diffraction analysis, the relative intensity of diffraction lines is measured by their density in the photographically-recorded diffraction pattern. In X-ray diffractometry a counter tube is substituted for the photographic film as a radiation detector. The number of quanta counted by the tube in unit time (counting rate) serves to indicate the relative diffracted intensity for a narrow Bragg angle region. The counter tube is mounted on a goniometer to permit scanning of the pattern.

A description of the "Norelco" X-ray diffractometer based on this principle was given in this Review some time ago [1]). In that article — hereinafter referred to as I — some general characteristics of the intensity measurements were discussed, e.g: the need for a very stable X-ray source; the reduction of the "background" of short wavelength continuous X-radiation by the use of an argon-filled Geiger counter tube which has a low sensitivity to these wavelengths; the accuracy limitation due to counting statistics; the inaccuracy of diffracted intensities due to the relatively small number of crystallites present in the specimen used; etc. Moreover, a number of methods available for performing the actual counting of the quanta and for recording the results were mentioned. The methods which can be selected in order to conform best to specific purposes will now be considered in greater detail. The means provided with the "Norelco" diffractometer for applying these methods will also be described. *Fig. 1* shows the cabinet containing all the circuitry and accessories used in X-ray diffractometry and also in X-ray spectrochemical analysis (to be dealt with in this Review shortly).

A short recapitulation of counting statistics will be included after a description of the first method; a general discussion of what may be called the "counting strategy" will be given following the description of the second method.

Point-by-point measurements with fixed time

A straightforward method consists of operating the counting device at a fixed Bragg angle position 2Θ of the goniometer for a predetermined length of time t, after which the number of counts N is read on a mechanical register. The procedure is repeated for the same time interval after moving the counter tube to another Bragg angle position, and so on. The counting rate

$$n = N/t \quad . \quad . \quad . \quad . \quad . \quad . \quad . \quad . \quad (1)$$

is computed and manually plotted against the angle read on the goniometer.

In view of the limited speed of the mechanical register, it is customary to "scale down" electronically the pulses delivered by the radiation detector before feeding them into the register. The scaling circuits used here are of a well-known binary type. Each stage therefore gives a reduction factor of 2. Eight such stages are provided with the "Norelco" diffractometer, enabling the selection of scaling factors 1, 2, 4, ... 128, 256 by press-button operation. The number of counts delivered by the detector is equal to the register reading multiplied by the selected scale factor. If required, interpolation between register readings is made readily by means of neon lamps included in each scaling stage which

*) Philips Laboratories, Irvington-on-Hudson, N.Y., U.S.A.

[1]) W. Parrish, E.A. Hamacher and K. Lowitzsch, The "Norelco" X-ray diffractometer, Philips tech. Rev. **16**, 123-133, 1954/55 (No. 4). For general information on diffraction analysis and diffractometry the reader may refer to: H. P. Klug and L. E. Alexander, X-ray diffraction procedures for polycrystalline and amorphous materials, Wiley & Sons, New York 1954; X-ray diffraction by polycrystalline materials, edited by H.C. Peiser, H. P. Rooksby and A. J. C. Wilson, The Institute of Physics, London 1955.

are lit by the even pulses and extinguished by the odd pulses arriving at each stage.

For good reproducibility, the counting time interval is controlled by a clock which is preset to the desired time period. A useful method consists of setting the fixed time interval (seconds) equal numerically to the selected scaling factor. In this case the number recorded on the mechanical register is equal to the counting rate in counts/sec. For time intervals exceeding 64 sec, counting must be controlled manually using a stop-watch.

Long counting time intervals are desirable in order to minimize the influence of the terminating errors of the clock ($^1/_5$ sec). At the same time, long counting periods decrease the error caused by the statistical fluctuations in the rate of arrival of the quanta at the detector. Since these fluctuations are of fundamental importance we shall expand on this point in the next section.

Straightforward though the point-by-point measurement and manual plotting may be, this method has the drawback that it makes an excessive demand on the operator's time. It can evidently be useful for scanning only a small portion of the diffraction pattern — and in fact the possibility of selecting small portions of a pattern for measurement constitutes one of the important features of diffractometry.

Fig. 1. Rack containing circuitry and accessories for the measuring and recording of diffracted X-ray intensities with the "Norelco" X-ray diffractometer.

Counting statistics [2])

Two measurements of a constant intensity, in which counting is performed during equal times t, will not in general yield the same number N of counts, owing to the random distribution of the quanta in time. A very large number of experiments would be required in order to obtain an average value N and the corresponding average value of the counting rate $n = N/t$ which is to be considered as a true measure of the X-ray intensity. The spread of the results N of individual experiments is approximately given (cf. Appendix) by a Gaussian distribution (*fig. 2*) of mean value N and standard deviation

$$\sigma = \sqrt{N} \quad . \quad . \quad . \quad . \quad . \quad . \quad . \quad . \quad (2)$$

An individual measurement N has a certain probability p of deviating from the true value by an amount $(N - N)$ smaller than a prescribed value ΔN_p. For the Gaussian distribution it can be shown that the "probable" error, i.e. the error ΔN_p for which $p = 50\%$, is

$$\Delta N_{50} = 0.67\sigma = 0.67\sqrt{N} \approx 0.67\sqrt{N}.$$

The probable *fractional* error ε_{50} of the calculated counting rate n is therefore

$$\varepsilon_{50} = \frac{\Delta n_{50}}{n} = \frac{\Delta N_{50}/t}{N/t} = \frac{0.67\sigma}{N} = \frac{0.67}{\sqrt{N}} \quad . \quad . \quad . \quad (3)$$

Thus, for example, 4500 counts are necessary to make $\varepsilon_{50} = 0.01$, i.e. to have a 50% probability that the result deviates less than 1% from the true value. In some cases a result giving a higher confi-

[2]) For a more extensive account of the statistics of counting and a bibliography, see : L. J. Rainwater and C. S. Wu, Nucleonics **1**, No. 2, 60-69, Oct. 1947; **2**, No. 1, 42-49, Jan. 1948.

dence in the prescribed accuracy is desired, with say $p = 90$ or 99%. This will necessitate longer counting intervals. The theory shows that

$$\varepsilon_{90} = \frac{1.64}{\sqrt{N}} \quad \ldots\ldots \quad (3a)$$

and

$$\varepsilon_{99} = \frac{2.58}{\sqrt{N}}, \quad \ldots\ldots \quad (3b)$$

so that about 27 000 counts are necessary to make $\varepsilon_{90} = 1\%$, and about 67 000 counts for $\varepsilon_{99} = 1\%$.

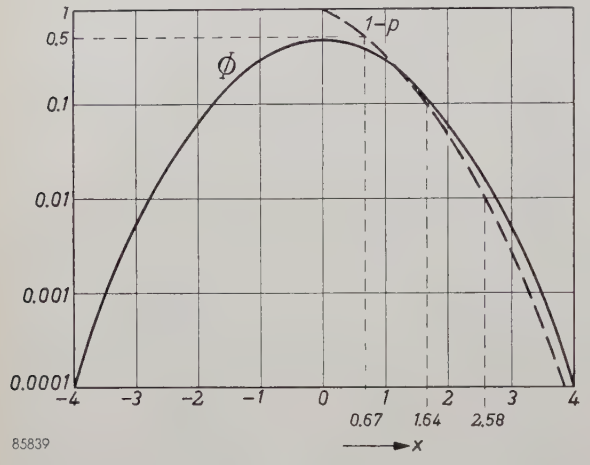

Fig. 2. Gaussian distribution function $\Phi = (1/\sqrt{2\pi}) \exp(-x^2/2)$. For a large count, $\Phi(x)dx$ gives the probability that the result will be between $\bar{N} + x\sigma$ and $\bar{N} + (x + dx)\sigma$, where $\bar{N}$ is the "true" value and σ is the standard deviation, $\sigma = \sqrt{N}$. The dotted curve, obtained by integration from the distribution function, shows $1 - p$, where p is the probability that the deviation of a count from the true value $\bar{N}$ is less than x times the standard deviation. For the probabilities $p = 50\%$, 90% and 99% the values of x are 0.67, 1.64 and 2.58 (see eq. 3, 3a, 3b). (From: L. J. Rainwater and C.S. Wu, loc. cit. [2]).

For these numbers of counts, ε_{50} is 0.4% and 0.26% respectively. *Fig. 3* is a graph of formulae (2), (3), (3a) and (3b).

The accuracy of an individual intensity measurement is considerably affected by the "background" of the diffraction pattern. If, at a certain Bragg angle, a total number of N pulses have been counted, while the background in the same angle region contributed N_B pulses in the same time, the diffracted intensity is calculated from $N - N_B$. The statistical error of this difference is given by

$$\sigma = \sqrt{\sqrt{N}^2 + \sqrt{N_B}^2} = \sqrt{N + N_B}$$

or

$$\varepsilon_{50} = \frac{0.67\sqrt{N + N_B}}{N - N_B}.$$

If $N = 500$ and $N_B = 0$, the error would be $\varepsilon_{50} = 3\%$. For $N = 600$ and $N_B = 100$, ε_{50} of the same resulting intensity is increased to 3.5% and for $N = 1000$, $N_B = 500$ it is increased to 5.2%.

It should be noted that the statistical error involved in point-by-point measurements will be markedly diminished in measuring the complete profile of a diffraction line, since a smoothed curve can generally be drawn through the individual measured points. The resulting error of an individual value, e.g. the peak intensity of the line, is difficult to assess but is certainly smaller than that given by (3). On the other hand, the errors discussed in this section refer only to the random arrival of the quanta and do not include possible errors due to instability of the X-ray source, finite resolving time of the counter tube and its circuits, and other causes, which will be briefly discussed at the end of this article.

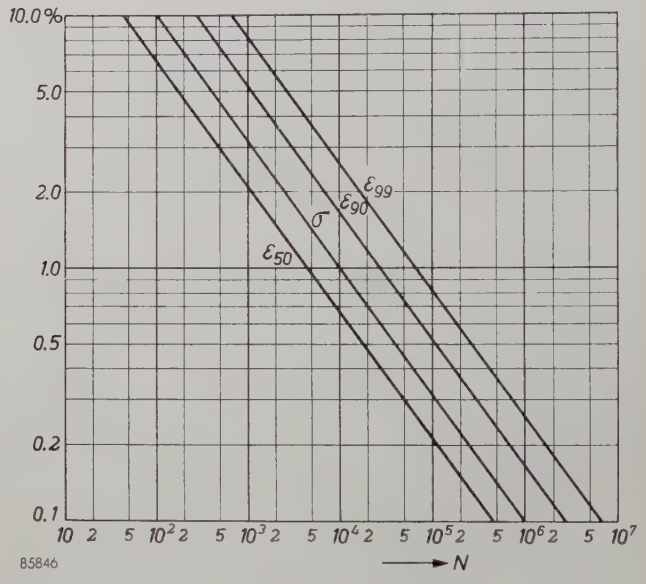

Fig. 3. Probable fractional error ε_{50} of counting rate, and 90% and 99% confidence limits ε_{90} and ε_{99}, as functions of the accumulated number of counts N, for a Gaussian distribution.

The recording counting-rate meter

Counting rates can be determined directly by measuring the mean value of the current composed of the separate counting pulses occurring in the detector. The basic circuit is illustrated in *fig. 4*. The voltage on the resistor R, which is smoothed by the condenser C, depends on the sum of the pulse current contributions received during the RC-time of the circuit. Since all pulses delivered to this circuit are of equal height and duration [3]), the voltage on R is a direct measure of the counting rate, averaged over about the RC-time.

[3]) In order to comply with this condition, averaging in the rate meter is preceded by equalizing the pulses in a pulse shaper.

Owing to the constant averaging time, the method is similar to the preceding one ("fixed time" measurements). Since the counting-rate meter is a direct and continuous indicating device, however, point-by-point measurement and plotting are no longer necessary. The detector is moved by the goniometer to scan the diffraction pattern *continuously*, while the rate meter reading is recorded on a strip chart moved synchronously with the goniometer. This combination of strip chart recorder (uppermost panel in fig. 1) and counting-rate meter is the most convenient and commonly used method in diffractometry since the operations are automatic and the accuracy is sufficient for the large majority of applications, such as qualitative chemical analysys, identification of surface layers, etc.

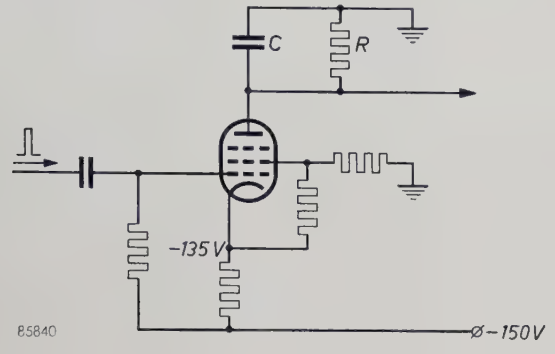

Fig. 4. Basic circuit of the counting-rate meter. The pulses arising in the counter tube are fed to the control grid of a pentode. Since the anode current of the pentode is nearly independent of the anode voltage, a constant charge is passed through the pentode for every pulse, independent of the charge already present on the capacitor C. The voltage produced across the resistor R is smoothed by C.

The accuracy of the relative intensity measurements obtained with the counting-rate meter is also subject to the fundamental limitation due to the statistical fluctuations. Measuring the counting rate n with the counting-rate meter which has a time constant RC can be shown to be equivalent to totalling the number of quanta arriving during a time interval $2RC$ (the operating time of the rate meter of course must be several times in excess of $2RC$ in order that this statement be valid). Thus, an individual counting-rate meter reading contains the probable fractional error

$$\varepsilon_{50} = \frac{0.67}{\sqrt{2n\,RC}} \quad . \quad . \quad . \quad . \quad . \quad . \quad . \quad (4)$$

As mentioned earlier, the statistical error will be greatly diminished by drawing a smoothed curve through the more or less ragged strip chart recording [4]). The resultant accuracy of a recorded pattern will depend hardly at all on the time constant but only on the total number of quanta detected during the recording, i.e. on the scanning speed and the width of the receiving slit of the counter tube.

Apart from this statistical error, the counting-rate meter will introduce a certain *distortion* of the line shape when the diffraction pattern is continuously scanned. This distortion is due partly to the width of the receiving slit just mentioned — an effect similar to that encountered in scanning photographically-recorded diffraction patterns with a microphotometer slit — and partly to the rate meter output lagging behind the input by a time roughly equal to the time constant RC [5]). The time lag effect evidently will be more noticeable the higher the rate of change of the counting rate, i.e., the steeper the profile of the scanned line and the higher the scanning speed. The distortion of the line shape results in a shift of the peak in the direction of scanning, a reduction of the peak height and an increase in the width of the line. These effects are demonstrated in *fig. 5a-c* which shows a diffraction line (a doublet) recorded with different scanning speeds. In each of the three cases illustrated, the line is first scanned in the direction of increasing Θ and then in the direction of decreasing Θ (this is easily effected by means of the limit stops on the goniometer which reverse the direction of scanning, see I). It will be noted that the recorded profile of the line differs considerably for the two scanning directions. This difference is due to the fundamental asymmetry of the diffraction line, caused by geometrical aberrations [6]) and by the overlapping of $K\alpha_1$ and α_2 lines. (With regard to the latter point, it should be remembered that the $K\alpha$ line of copper or of whatever target material is used in the X-ray tube, consists of a doublet, the two components α_1, α_2 differing slightly in wavelength and producing two superimposed diffraction patterns; the α_1 and α_2 lines will overlap at small Bragg angles and be separated at large angles.)

In fig. 5*a* to *c* progressive deterioration of the line shape is caused by increasing the scanning speed. The same deterioration occurs when using a fixed scanning speed but increasing the time constant of the rate meter: see *fig. 6a-c*. In fact both effects are equivalent and the distortions in the chart recording

[4]) See: H. S. Peiser, H. P. Rooksby and A. J. C. Wilson, l.c. [1]), p. 223.

[5]) W. Parrish, E. A. Hamacher and M. Gabin, Amer. Cryst. Assoc. Meeting, Penn. State College, 11 April 1950. M. Tournarie, J. Phys. Radium (Supp. No. 1) **15**, 16A-22A, 1954.

[6]) These include the effect of the "line" being ring-shaped, the so-called flat-specimen error and others, which cannot be discussed further here (see I, and A. J. C. Wilson, J. sci. Instr. **27**, 321-325, 1950).

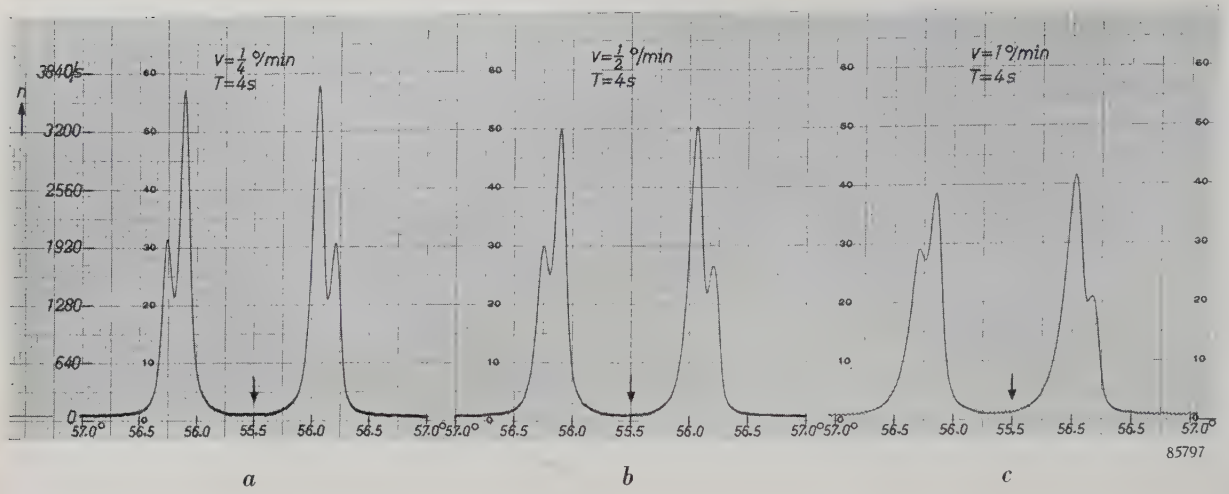

Fig. 5. *a-c*) Diffraction line (silicon, reflecting plane 311) recorded with the counting-rate meter at three different scanning speeds v; time constant $T = 4$ seconds. Unfiltered CuK radiation, angular aperture 1°, receiving slit width 0.15 mm.
Each recording shows the line scanned in both directions (reversal of direction at the arrow). The line profile is seen to deteriorate as the scanning speed is increased. The speed of the recorder chart, which can be varied independently of the goniometer speed v, was selected to make the width of the recordings *a*) - *c*) equal. The number of counts accumulated in any given angular interval naturally decreases with increasing v.

depend only on the *product* of scanning speed and time constant. This can be seen by comparing the line profiles of fig. 5*a* with 6*a*, 5*b*-6*b* and 5*c*-6*c*. Each pair of recordings was obtained with different time constants and scanning speeds, their product, however, being identical.

The resulting distortion of the profile of a particular line (Si 111, CuKα radiation) recorded with a receiving slit of 0.15 mm width, is shown quantitatively in *fig.* 7, where the peak value I_p, the peak shift $\Delta 2\Theta$ and the line width W at one-half peak height are plotted against the product (time constant) $\times$ (scanning speed).

The time constant may be varied in the "Norelco" diffractometer by selecting one of a set of capacitors C in the rate meter circuit (fig. 4). A number of scanning speeds, viz. $^1/_8$, $^1/_4$, $^1/_2$, 1 and 2° (2Θ) per min, can be selected by the use of changeable spur gears in the goniometer drive (cf. I). For general powder diffraction problems a scanning speed of $^1/_4$° per minute and time constant 4 sec have proved most satisfactory. The peak shifts are then less than 0.01° (2Θ) so that peak position corrections (from a table giving correction as a function of Bragg angle) are usually unnecessary. A smaller time constant will decrease the peak shift and other distortion but

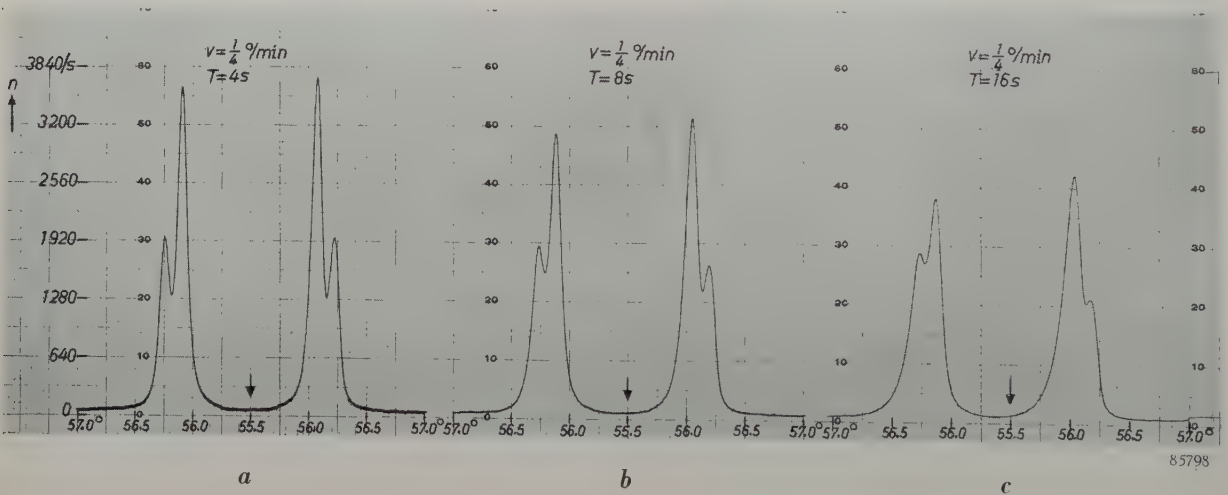

Fig. 6. *a-c*) The same diffraction line as in fig. 5, recorded with the counting-rate meter at a scanning speed $v = \frac{1}{4}$° per min and three values of the time constant T. All other conditions same as in fig. 5. Note that the deterioration of line shape with increasing T is similar to that in fig. 5. The number of counts in corresponding angular intervals, however, is the same for all three recordings.

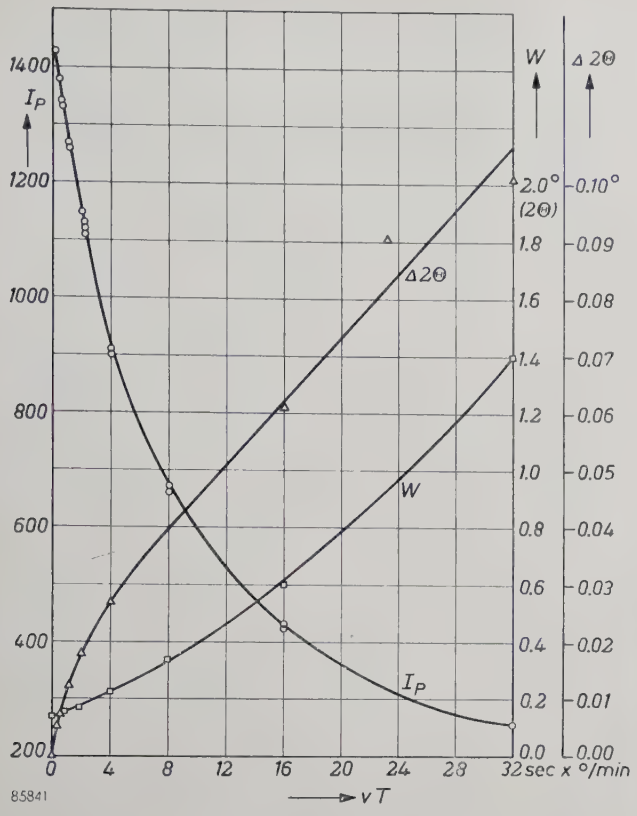

Fig. 7. Effect of the line distortion caused by scanning speed v and time constant T, on the peak height I_P (after subtraction of the background intensity I_B), the angular peak location (shift $\Delta 2\Theta$) and the with W at one-half peak height. The effects depend only on the product vT. These measurements were made on the Si 111 line with CuKα radiation (Kα doublet not resolved) and receiving slit width 0.15 mm. The curves are valid only for the specified experimental conditions and will vary with line shape and receiving slit width. Lines with similar profiles in the same pattern, will be affected by the same percentage peak reduction and therefore need no further correction.

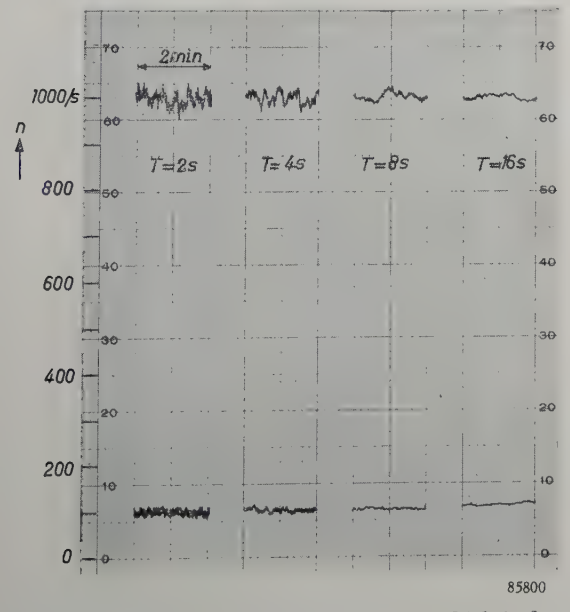

Fig. 8. The "jitter" of the recorded trace, which is due to the statistical fluctuations of the counting rate, diminishes with increasing time constant T. The recordings shown were made at a fixed position of the detector, with counting rates $n = 1000$/sec and $n = 100$/sec.

increase the "jitter" of the recorded trace. This is seen in fig. 6 and is demonstrated more clearly by *fig. 8*. A higher scanning speed, although desirable for more efficient use of the equipment and of the operator's time, will affect the accuracy of the intensity values as was shown above. The effect may be compensated by using a wider receiving slit, thus restoring the total number of counts to the original level. This procedure is frequently employed for rapid surveys of diffraction patterns which are not too complicated, i.e. where the loss in angular resolving power (and the reduced peak to background ratio, see fig. 18) due to the wider slit can be tolerated. The difference in appearance between a recording made for good accuracy and a recording made for a rapid survey is shown in *fig. 9*.

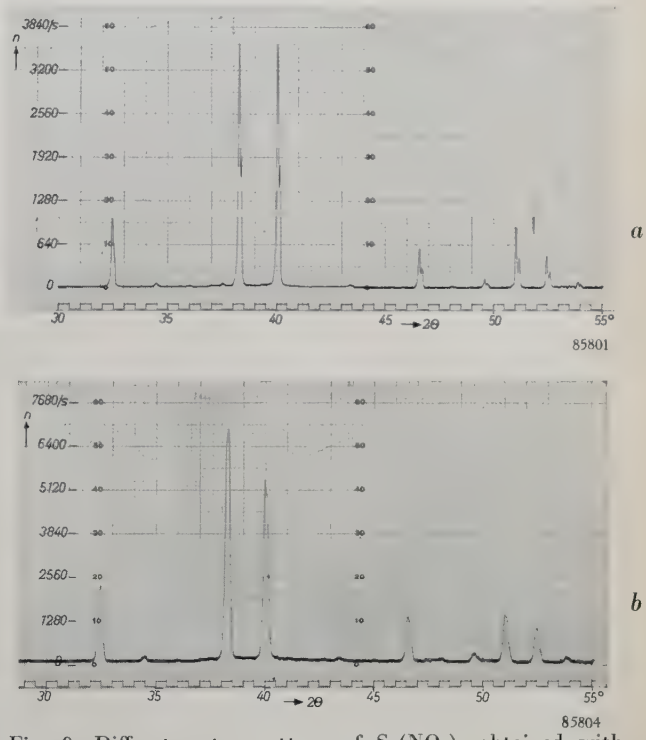

Fig. 9. Diffractometer pattern of $Sr(NO_3)_2$ obtained with CuKα radiation, 30 kV peak, 20 mA.
a) Recorded with 0.15 mm receiving slit at scanning speed $v = \frac{1}{4}°$/min and with time constant $T = 4$ sec.
b) Recorded with 0.60 mm receiving slit, $v = 1°$/min and $T = 2$ sec.
The total number of counts is approximately the same in both cases (92 290 and 88 260 respectively, after subtraction of background), but the angular resolution of record (*b*), which took only $\frac{1}{4}$ of the time necessary for (*a*), is much poorer. Peak-to-background ratio for (*a*) 96.5, for (*b*) 42.7 (cf. fig. 18).

It should be pointed out that the errors inherent in continuous scanning with a device which is subject to a time-lag can be greatly reduced by scanning step-wise and stopping at every step for a period several times longer than the *RC*-time. The "Norelco" goniometer is provided with a step-scanning device (see I). The resulting line profile, corresponding in accuracy to a profile measured at very low continuous scanning speed, is illustrated by *fig. 10*.

A novel feature of the "Norelco" counting-rate meter is its relatively small basic range, the full scale deflection corresponding to 50 counts/sec. In order to cover a wide range of intensities, the impulses delivered by the detector are scaled down by the binary scaling circuits mentioned above

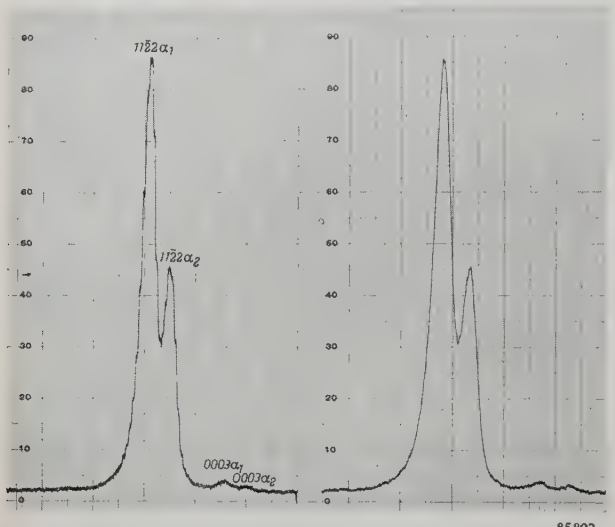

a *b*

Fig. 10. Diffraction lines (quartz 1122 and 0003) recorded with the counting-rate meter: *a*) step scanning with 0.02° steps, counting time interval for each step 30 sec, time constant $T=$ 4 sec; *b*) continuous scanning at $v = {}^1/_8{}^\circ$ per min.

before being applied to the rate meter. Thus the full scale range of the ratemeter can be adjusted from 50 to 12 800 counts/sec by exact factors of 2. An additional switch changes the basic range to 0.8×50 and to 0.6×50 counts/sec, so that there are 27 full scale ranges available. The advantage over the usual wide-range type of rate meter is that greatly differing relative intensities (recorded on different ranges) may be accurately compared. Moreover, calibration is simplified by using the power line frequency (mains frequency) as a standard for any of the three basic ranges; all other ranges are automatically calibrated by multiplication by exact factors of 2.

Another advantage of scaling the pulses down before averaging is that higher counting rates can be precisely measured, since counting losses caused by the finite resolving time of the actual counting circuit will be reduced (see the section on Linearity at the end of this article). This favorable influence of the scaling-down procedure is enhanced by its so-called regularizing effect: the scaled down pulses arriving at the counting circuit are more regularly spaced than the original ones, so that their number per second without undue losses may approach more closely the critical frequency existing for a strictly periodic sequence [7]).

[7]) Cf. e.g. E. J. van Barneveld, Fast counter circuits with decade scaler tubes, Philips tech. Rev. **16**, 360-370, 1954/55 (No. 12).

The rate meter circuit is designed so that its output can be combined with that of an additional rate meter to give a voltage proportional to either the sum, the difference or the ratio of two intensities measured. Only one recorder is needed to record this composite result. Such a facility is useful for various monitoring techniques.

The "counting strategy"

The dependence of the accuracy on the accumulated number of counts, see eq. (2) and (3), is the factor dominating all intensity measurements made with Geiger tubes or other counter tubes [8]). One consequence is that when using *fixed* time intervals for counting — as in the methods described above — the relative error is inversely proportional to the square root of the counting rate, i.e. of the intensity.

The question arises whether or not this "natural" variation of accuracy with intensity should be accepted or not. Different variations of accuracy with intensity can obviously be obtained by using *variable* time intervals for counting. In order to answer the above question, the final use that has to be made of the recorded intensities must be taken into account. Two main cases will be considered.

a) For some problems, *ratios* of intensities must be calculated to yield the solution. This applies to the study of strain in cold-worked metals, of particle size distribution, e.g., in clay minerals, of imperfect structure in crystals, etc., where broad diffraction lines are found; information in these cases is obtained from a Fourier expansion of the line profile, whose exact form ("local" relative intensity at each angle) should then be precisely measured [9]). It also applies to quantitative chemical analysis, where the ratio of the percentages of components in a mixture is proportional to the ratio of the intensities (peak values) of their respective diffraction lines. In these cases the local (or peak) values which constitute the numerator and denominator of the ratio to be computed, should be known with approximately the same *relative* accuracy: decreasing the relative error in only one of them will not significantly improve the accuracy of the ratio.

[8]) Strictly speaking, it is also present in photographic intensity measurements but the enormous number of quanta involved renders the statistical error so much smaller than the errors caused by the techniques of density measurements, that it was overlooked for a long time. Only recently, with the advent of X-ray image intensifying devices in which quanta effects are preponderant, have investigators grown more aware of the role of these effects in photographic recording (see e.g. Philips tech. Rev. **17**, 71-77, 1955/56, No. 3).

[9]) B. E. Warren and B. L. Averbach, X-ray diffraction studies of cold work in metals, Chap. V in Imperfections in nearly perfect crystals, Wiley & Sons, New York 1952; A. J. C. Wilson. X-ray optics, Methuen & Co., London, 1949.

For this type of problem, therefore, the counting strategy should be such that a constant relative error is obtained at all counting rates. From eq. (3) it is seen that to attain this result a *fixed number N of counts* has to be accumulated at every Bragg angle position. This is equivalent to making the counting time inversely proportional to the counting rate; see *fig. 11.*

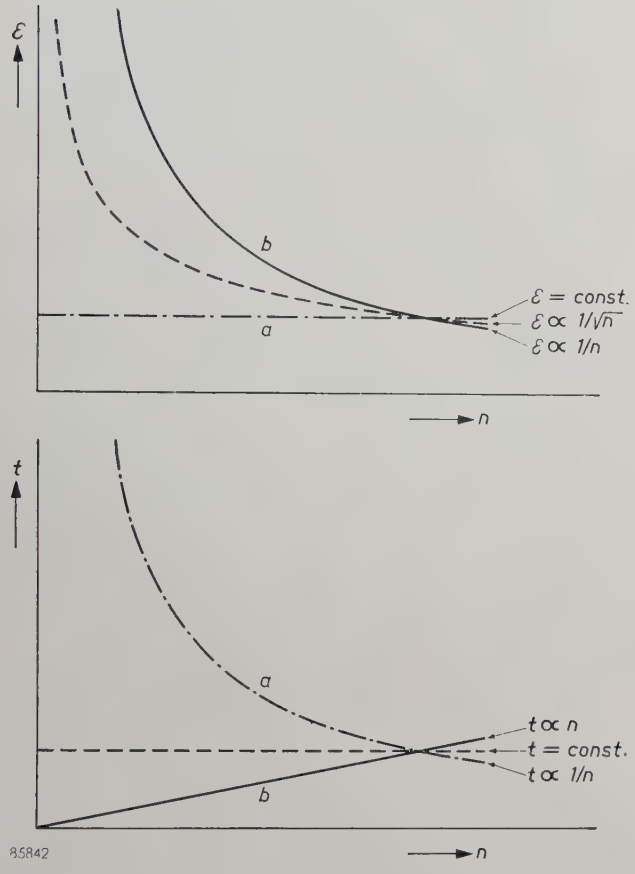

Fig. 11. The relative statistical error ε and required counting time t, as functions of the counting rate n, for three different types of counting strategy.

b) in every measurement of a single peak intensity, the *difference* of two counting rates has to be calculated, viz. that between peak and background. In this case, these two counting rates should be known with approximately the same *absolute* accuracy: decreasing the absolute error in either of them will only slightly improve the accuracy of the difference.

A constant absolute accuracy will also be desirable in ascertaining the profile of a line, when the relative error has been decreased to a degree where the absolute error is equal to that due to the width of the line written by the recorder. The width, of course, will affect all local intensity values by a constant absolute error (about 0.2% of the recorder range).

In order to obtain a constant absolute error at all counting rates, i.e., a relative error inversely proportiona to the counting rate, $\varepsilon \propto 1/n$, the counting time t must be made *proportional to the counting rate*, as is seen from eq. (3) and (1). This is also illustrated by fig. 11.

The "natural" counting strategy, using fixed time intervals for counting, regardless of the counting rate, stands in between cases (*a*) and (*b*). The situation is summarized in *Table I.*

Table I. Different types of "counting strategy".

	Dependence of relative error ε on counting rate n	Dependence of counting time t on counting rate n
Constant relative error ("fixed count", case *a*)	$\varepsilon = \text{const.}$	$t \propto \frac{1}{n}$
Fixed time	$\varepsilon \propto \frac{1}{\sqrt{n}}$	$t = \text{const.}$
Constant absolute error (case *b*) . . .	$\varepsilon \propto \frac{1}{n}$	$t \propto n$

The realization of case (*b*), to our knowledge, has never been attempted in an automatic recording instrument. Case (*a*), on the other hand, represents the well known "fixed count" method. Ways of applying this method will be described in the next sections.

It should be pointed out that still other varieties of counting strategy are conceivable and have been used. The method described by Cooke-Yarborough is such a variety [10]), compromising between the fixed count and the fixed time methods.

The above statements concerning the effect of statistical errors on the ratio and on the difference of two measured values can be understood as follows.

If two counting rates n_1 and n_2 ($n_1 > n_2$) have the relative errors ε_1 and ε_2, the absolute errors are $n_1\varepsilon_1$ and $n_2\varepsilon_2$ (it does not matter whether the "probable" errors ε_{50} or the 90% or 99% confidence limits ε_{90} or ε_{99} are considered).

The relative errors ε_r of the *ratio* n_1/n_2 and ε_d of the *difference* $n_1 - n_2$ will be:

$$\varepsilon_r = \sqrt{\varepsilon_1^2 + \varepsilon_2^2},$$

$$\varepsilon_d = \frac{\sqrt{\varepsilon_1^2 + \left(\frac{n_2}{n_1}\varepsilon_2\right)^2}}{\left(1 - \frac{n_2}{n_1}\right)}.$$

If ε_1 is fixed, it is seen that in both cases the second term under the root should not be appreciably larger than ε_1^2, since this would greatly increase the resulting error (the latter can be visualized as the hypotenusa of a right-angle triangle). On the other hand, little profit is gained by making the second term much smaller than ε_1^2, since in that case the resulting

[10]) F. H. Cooke-Yarborough, The counting of random pulses, J. Brit. Inst. Radio Eng. **11**, 367-380, 1951.

error would remain approximately equal to ε_1. A suitable procedure, therefore, is to make the second term approximately equal to the first. Thus for the ratio, it is desirable to have $\varepsilon_2 \approx \varepsilon_1$ (equal relative errors of both counting rates) and for the difference it is desirable to have $n_2\varepsilon_2 \approx n_1\varepsilon_1$ (equal absolute errors).

In a more rigorous treatment of the problem [11]), one would have to take into account that a decrease of ε_2, the error of the smaller of the two counting rates, will require a greater expenditure in time than an equally important decrease of ε_1. The most "economic" proposition would be to ensure that a small improvement in ε_r (or ε_d) would cost the same additional counting time whether it be achieved by decreasing ε_1 or by decreasing ε_2. A simple calculation shows that the counting time would have to be chosen proportional to the square root of the counting rate in order to meet the said requirement for ε_r, and inversely proportional to the square root of the counting rate in the case of ε_d.

Point-by-point measurements with fixed count

Point-by-point measurement of a diffraction pattern according to the "fixed count" method is performed in the following manner: in each goniometer position, the clock-type mechanical register actuates a count stop circuit after it has made 100 steps, i.e. after one complete revolution of the main pointer. Thus the scaling circuits are in operation for the time necessary to accumulate a predetermined number of counts N, viz., 100, 200, ... 12 800 or 25 600, and the time interval t is measured by an electric stop clock (*figs. 12* and *13*). The value t is used to calculate the counting rate $n = N/t$, which can then be plotted against the Bragg angle.

Because the number of counts is preselected at a fixed value, the relative accuracy of all measured intensities will be equal and have a preselected value (eq. 3). Of course the method has the same disadvantage of being time-consuming as the point-by-point measurement with "fixed time" counting. In fact the disadvantage is even more pronounced because the time required for each measurement varies with the intensity and becomes very long at low counting rates (fig. 11). We must not complain of this peculiarity of the method, however, since it really represents *le défaut de ses merites*, and its

[11]) The following considerations were pointed out to us by Dr. H. C. Hamaker of the Philips Laboratory at Eindhoven. We are also indebted to Dr. P. M. de Wolff of the T.N.O., Delft, for general suggestions concerning the comparison of counting stategies.

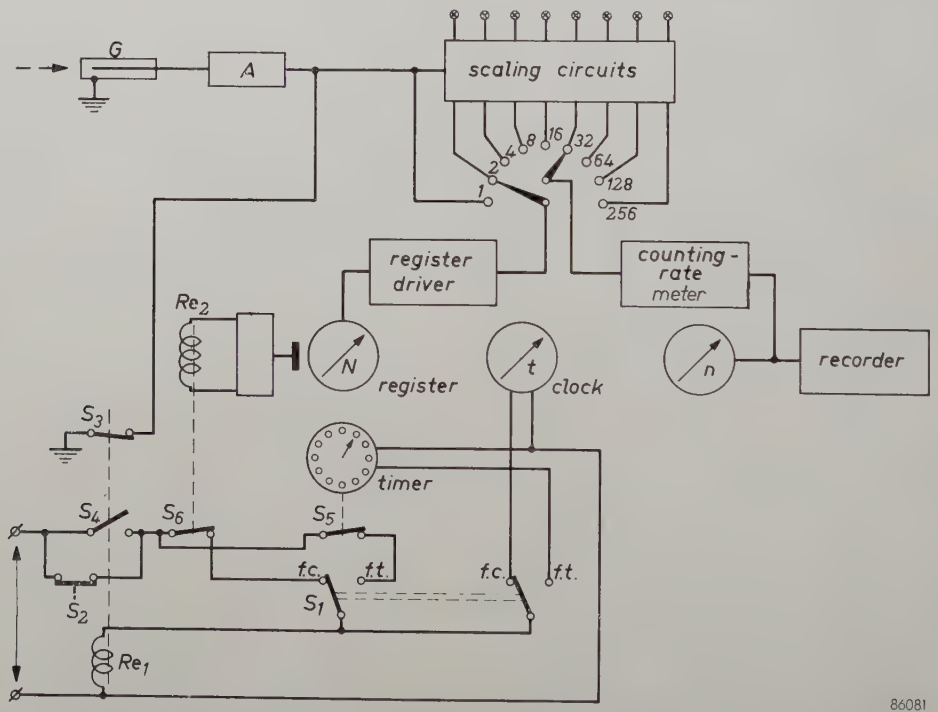

Fig. 12. Schematic block diagram of circuits for measuring intensities by different methods. The pulses produced in the detector G (e.g., a Geiger counter tube) pass through a pulse shaper and amplifier A to the scaling circuits consisting of eight binary stages. *Fixed time methods:* Pulses from any selected stage of the scaling circuits are counted in the register N for a time selected on the timer by setting the operation selection switch S_1 to position f.t. ("fixed time"). The measurement begins by pressing push button S_2; this will start the timer and energize relay Re_1 which closes the holding contact S_4 and opens switch S_3, so that counts are passed from the amplifier to the scaling circuits and the register. After the preset time, the timer opens switch S_5; this de-energizes Re_1, closes S_3 and opens S_4, thus stopping the operation. For making a rate meter recording, S_2 is kept closed by means of another switch (not shown) parallel to the push button so that counting continues indefinitely. If the limit switches on the goniometer are used, they actuate microswitches (not shown) which operate S_2. *Fixed count methods:* Selector switch S_1 is switched to position f.c. ("fixed count"). This measurement again begins by pressing S_2. When the main pointer of register N has completed one revolution, a contact (not shown) is closed, relay Re_2 is energized via a relay tube, so that switch S_6 opens and relay Re_1 is de-energized, thus completing the cycle. The counting rate is calculated from the time on the clock which starts and stops simultaneously with the register.

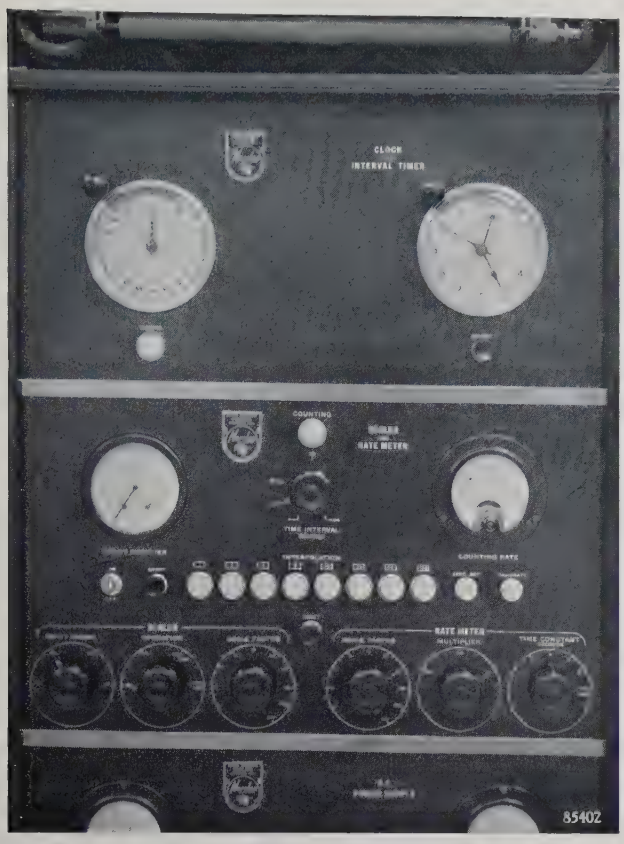

Fig. 13. Front view of the panels which contain the scaling and rate meter circuits (below, cf. also fig. 1), the interval timer and clock (above).

sting can be removed by applying the device described in the following section.

The counting-rate computer

To eliminate the labor involved in making accurate intensity measurements with the fixed count method, the "Norelco" counting-rate computer has been developed [12]). This device automatically performs the sequence of operations required and records the data. It will be described at some length in an article in the next issue of this Review, and only its basic characteristics and performance will be mentioned here.

The computer chassis is about the size of the scaling circuit chassis and fits in the electronic circuit rack in place of the clock and interval timer (fig. 1, second panel from top). The computer is of the analogue type; it is based on Ohm's law and delivers an electric current inversely proportional to the time required to accumulate a predetermined number of counts, at a given Bragg angle position of the detector. This current is fed to the strip chart recorder so that a plot of the counting rate (on a linear scale) is obtained on the recorder. After one value has been recorded, the instrument advances the chart a fixed increment, advances the counter tube a fixed angular increment and then starts the counting circuits automatically to repeat the cycle. A step-wise recording is obtained in this way. The angular increment may be selected as 0.01°, 0.02° ... 0.05° (2Θ). The statistical error (total number of counts for one position) and full scale intensity are also selectable.

A typical recording obtained with the counting rate computer is shown in *fig. 14*. About $2\frac{3}{4}$ hours was required to record the pattern in the limited Bragg angle region shown, but the operation was entirely automatic.

The Cooke-Yarborough method

In fixed count measurements, time consumption is largest for the lowest intensities and especially for the background. The desirability of not spending too much time on one recording (though it may be only instrument time) has led to the development of several modified "fixed count" methods, which sacrifice some of the accuracy at the lower intensities. One method consists of increasing the angular increment when scanning regions containing only the background. For example, steps of 0.05° could be used in such regions and 0.01° for the lines. Another method is to reduce the scaling factor for the background measurements, thereby increasing their relative statistical error. Both methods can be combined, but the gain in speed is limited by the "recycling time" of the computer, i.e., the time not required for the actual counting but for the recording and the chart and goniometer movement. This shows that the first-mentioned expedient (increase of step width) is more effective since it diminishes the number of

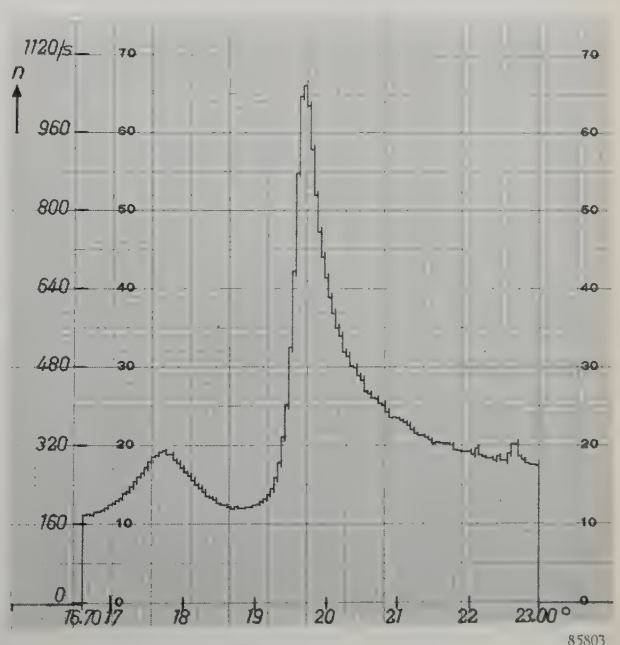

Fig. 14. Part of recording of a diffraction pattern ($16.7° < 2\Theta < 23.0°$) made with the counting rate computer. Montmorillonite (dry specimen), CuKα radiation with nickel filter, steps 0.05° with $N = 6400$; recording time $2\frac{3}{4}$ hours.

[12]) W. Parrish and E. A. Hamacher, Geiger counter X-ray diffraction spectrometer: instrumentation and techniques, Trans. Instr. Meas. Conf. Stockholm 1952, p. 95-105.

recycling periods; the second method, moreover, has the drawback of changing the amplitude recorded on the chart paper.

Both modifications have the disadvantage of requiring the operator's attention to change scale factors or angular increments at the appropriate time. To avoid this and to return to completely automatic operation, the method devised by Cooke-Yarborough [10]) may be employed. He recommended adding periodic pulses at a constant, controlled, low rate to the random pulses that are to be measured. At high counting rates the added pulses, say 100 per second, hardly play a role so that the high and uniform relative accuracy characteristic of the fixed count method will remain unaffected in measuring the peaks. At low counting rates the time required for a measurement (i.e., for accumulation of the preselected number of counts) obviously approaches a fixed value, dependent upon the added constant pulse rate. The Cooke-Yarborough method therefore stands between the fixed count and the fixed time counting methods.

When using the Cooke-Yarborough method in conjunction with the counting-rate computer, it is an important consideration that the intensity scale should remain linear. It will be shown in the article on the computer that this is obtained by selecting a pulse rate, f, which is a fixed fraction, x, of the full scale counting rate: $f = x(n + f)_{max}$. A pulse generator has been designed which is synchronized with the power line and delivers pulses on a basis of $x = 0.075$, so that for $(n + f)_{max}$ varying from 50 to 3200 counts/sec (the upper limit for the computer) pulse frequencies of 3.75, 7.5, ..., 240/sec are provided.

The gain in time can be seen by referring to *fig. 15*. The dotted lines show the time required in normal operation for accumulating the predetermined number of counts $N(= 100 \times$ scale factor), as a function of the counting rate (X-ray intensity), for different values of N. The minimum time, being equal to 8 sec for all values of N, corresponds to the maximum output current of the computer. The solid curves show the time required by the Cooke-Yarborough method with $x = 0.075$. The time at low counting rates is considerably reduced and approaches a maximum of 106.6 sec in all cases. The time for the highest counting rates is not greatly affected: it is decreased from 8 to 7.45 sec.

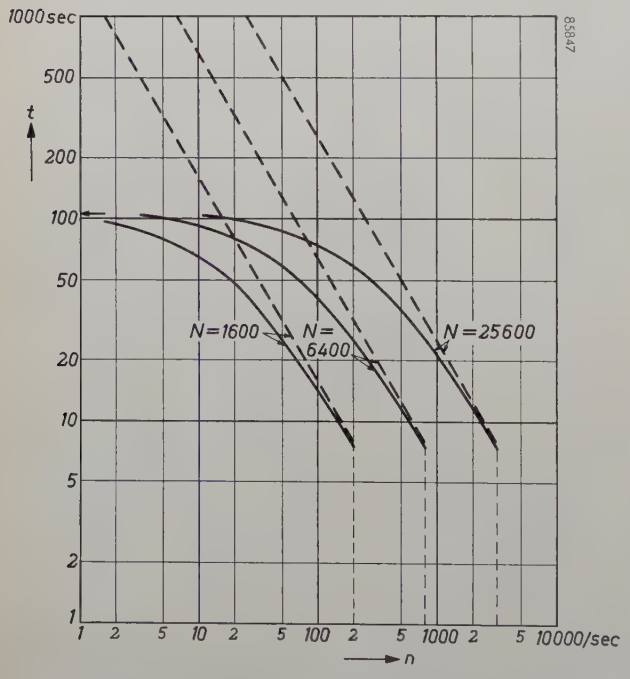

Fig. 15. Time t required to accumulate a number of counts N, in normal operation (dotted lines) and in the Cooke-Yarborough method (solid lines). The added pulse frequency f is 0.075 times the full scale counting rate.

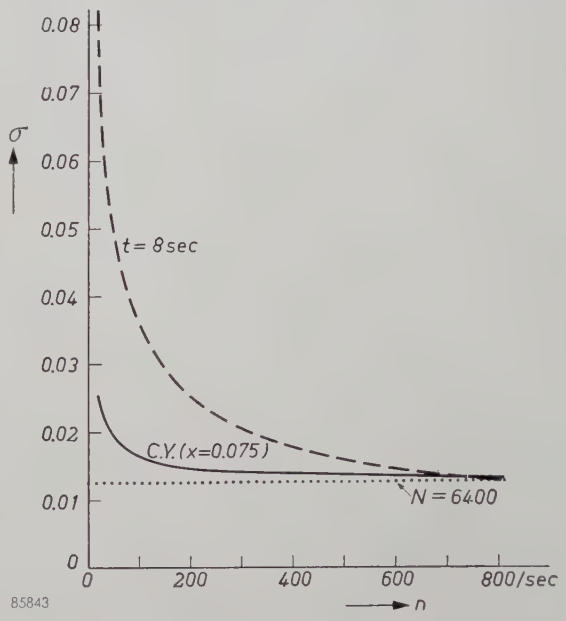

Fig. 16. The standard deviation σ as a function of the counting rate n, for the Cooke-Yarborough method (C.Y.), for fixed time measurements with $t = 8$ sec (— — —) and for fixed count measurements with $N = 6400$ (. . . . .).

The actual time required to scan a given portion of a diffraction pattern will depend upon the background level and the number of lines and their intensities. In one specific case, the counting-rate computer required 8 hours to record a pattern which included a sharp line profile and a large background region; the use of the Cooke-Yarborough method reduced the time for the same pattern by a factor of about 2. The expected saving in time is not fully realized because of the recycling time of the computer (see above) which amounts to 60 sec per cycle.

The loss in statistical accuracy involved by the Cooke-Yarborough method must also be considered. The standard deviation with this method is [10]):

$$\sigma_{C.Y.} = \frac{1}{\sqrt{N}} \sqrt{\frac{n+f}{n}} \quad . \quad . \quad . \quad . \quad . \quad . \quad (5)$$

$\sigma_{C.Y.}$ as a function of n, for $f = 60$ and $N = 6400$ (range $(n + f)_{max} = 800$) is shown in graphical form in *fig. 16*; the σ-lines for normal fixed count operation ($N = 6400$) and for fixed time operation (8 seconds) are drawn in for comparison. The Cooke-Yarborough modification resembles fixed time operation in that as the counting rate decreases the relative statistical error increases. At high counting rates, all three methods give essentially the same statistical accuracy.

Integrated intensity measurements

The peak height of a diffraction line is often tacitly assumed to represent the line intensity. Although quite satisfactory and convenient for the routine identification of substances, peak heights are

less suitable for precise quantitative analysis. For this purpose, the "line intensity" should be a quantity strictly proportional to the percentage of the substance present. We have seen that this is not the case for the peak height, which in rate meter recordings is markedly dependent upon the scanning

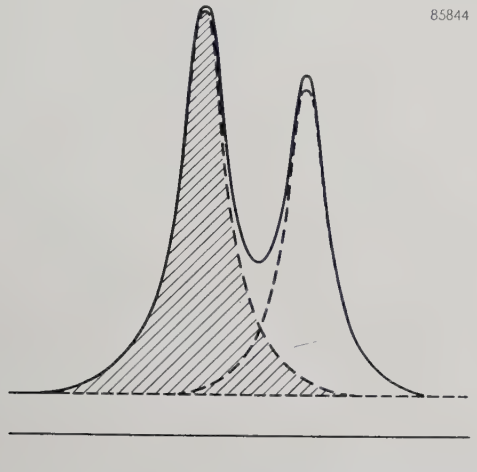

Fig. 17. The area of slightly overlapping diffraction lines reflected from different lattice planes can be integrated by sketching in the "tails" of the lines in the overlapping region and using a planimeter.

speed and even upon the scanning direction. A quantity which physically represents the line intensity more correctly is the total diffracted energy, i.e. the intensity integrated across the entire width of the diffraction line. This integrated intensity (area of a diffraction line) is not affected by the distortion of line profile and change of peak height inherent in the rate meter recording [12]). It is also of importance for structural analysis, since the line intensity thus defined is directly related to the structure of the crystal.

Practical considerations which favor the use of integrated intensities are the following: 1) the statistical error inherent in the measurement of the area of a line is smaller than that in the measurement of the peak, owing to the much larger number of counts summed; 2) the problem of the overlapping of $K\alpha_1$ and $K\alpha_2$ lines is avoided. In the overlapping region the measured peak height of a line will be larger than the α_1-peak height (which is about double the α_2-peak height) by a factor which depends upon the extent of overlap. On integrating the line intensity, the total area including the α_1 and the α_2 contributions is always taken, so that it does not matter whether α_1 and α_2 are separated or not.

Table II, which lists the relative values of integrated intensity and of peak intensity of a few lines of one specimen, illustrates the effect of the α_1 - α_2 separation.

Of course, integration is only possible where there is no severe overlapping of lines reflected from different lattice planes. In cases of slight overlapping, the "tails" of the lines may be sketched in as shown in *fig. 17*. The integration is then performed by means of a planimeter. If no overlapping occurs, a very easy method is to use a receiving slit wide enough to include the entire line and count at the peak position (*fig. 18*). For a total line width of $0.01°(2\Theta)$, a 1.2 mm slit would be required. Another easy possibility for performing integrated intensity

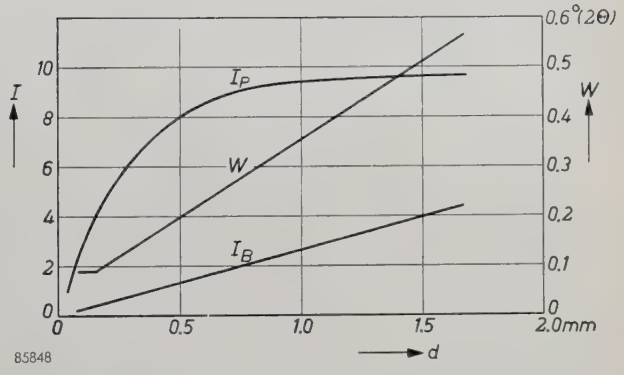

Fig. 18. When a diffraction line is scanned with receiving slits of increasing widths d, the recorded peak intensity I_P (with background subtracted) also will increase. When the receiving slit becomes wider than the line, the intensity no longer increases and the peak value indicates the integrated line intensity. The background I_B and the width W (degrees 2Θ at half peak height) of the recorded line profile continue to increase with receiving slit width. These curves were obtained using the 111 line of silicon with Cu Kβ radiation using an angular aperture $2\alpha = 1°$. Wider lines and Kα-doublet separation will change the given values.

Table II. Comparison of area and peak height of a few silicon lines to show influence of $K\alpha_1$-α_2 separation. Unfiltered CuK radiation was used with an angular aperture of 1°; receiving slit width 0.15 mm; scanning was done with speed $\frac{1}{4}°(2\Theta)$ per min, time constant 4 sec, scaling factor 128. All values have been corrected for the background.

Line	2Θ - range	Total number of counts (area of line)	Counting rate at peak of line counts/sec	Relative intensity derived from	
				area	peak
111	29.5 - 27.5°	48 040 ± 0.5%	$\alpha = 1336 \pm 0.5\%$	100	100
220	48.5 - 46.5°	36 590 ± 0.5%	$\alpha_1 = 903 \pm 1.1\%$	74.0	67.6
331	57.0 - 55.0°	21 376 ± 0.8%	$\alpha_1 = 511 \pm 0.9\%$	44.4	38.3

measurements is provided with the "Norelco" equipment. The goniometer scans the pattern continuously, and the scaler is started manually at one side of a line and shut off after the line has been scanned. During scanning, the mechanical register sums the counts, the total number being proportional to the area of the scanned portion of the pattern.

The integrated background intensity should of course be subtracted. This is measured separately, for example by counting the total number of background pulses in a region adjacent to the line and of the same width as the scanned line. It is also possible to correct in a simple way for a background which varies slowly with the angle.

In cases were the line is weak it may be scanned back and forth several times to accumulate sufficient counts for the desired statistical accuracy.

When the relative intensities of two or more lines are to be compared, the same receiving slit width and scanning speed must be used or allowances made for any differences in these factors.

It was stated above that the area of a line is more suitable than the peak height for representing the line intensity. Similarly for the exact angular position of a line, the *center of gravity* defined by

$$2\Theta_1 = \frac{\int n \times 2\Theta \, \mathrm{d}(2\Theta)}{\int n \, \mathrm{d}(2\Theta)} \quad . \quad . \quad . \quad . \quad . \quad . \quad (6)$$

is a better indication than the angular peak position. Since the measured line profiles are unsymmetrical and the peaks have a finite breadth, there is always some doubt about how to define the precise position of the peak; these doubts do not interfere with the determination of the center of gravity. Moreover, the effect of the most important systematic errors (which depend on the Bragg angle 2Θ and which have been calculated) can be easily allowed for with the center of gravity, whereas the corrections for the peak positions are so complicated they have been worked out for only a small angular region [13]). The center of gravity is readily calculated from a counting rate computer record, and although this procedure takes considerable time, it is useful in the determination of lattice parameters and other cases where the highest precision is required.

Incidentally, eq. (6) demonstrates that the angular accuracy depends on the accuracy of the intensity measurements. In a typical case, an accuracy of a few thousandths of a degree was obtained when measuring the intensities to an accuracy of $\varepsilon_{50} = \pm 0.8\%$, in 0.01° to 0.05° steps, across lines in the back reflection region. (The goniometer is also capable of setting and reading separate angles to this accuracy.)

Linearity of intensity measurements

All the above methods of mapping the intensity vs. angle relation are based on a linear relationship between diffracted X-ray intensity and number of counts. As pointed out in this Review on previous occasions [7]) [14]), such a linear relationship, even when background counts due to undesired radiation have been subtracted, exists only to a limited extent. Non-linearity is caused by the "dead time" of the detector and of the scaling circuit, which prevents quanta arriving within too short a time interval from being counted separately ("counting loss"). The resolving time of the Geiger counter tube (type No. 62019) usually used in the "Norelco" diffractometer is 170 microseconds. The effective resolving time when using the counter for detecting Cu Kα radiation produced by a 35 kV peak full-wave rectified X-ray source [15]) was found to be $\tau = 270$ μsec. This was established by measuring the response of the Geiger counter (observed counting rate n) to a known X-ray intensity (true pulse rate n_0); the response should obey the well-known relationship

$$n = \frac{n_0}{1 + \tau n_0} \quad . \quad . \quad . \quad . \quad . \quad (7)$$

The measured response is plotted in *fig. 19*. This

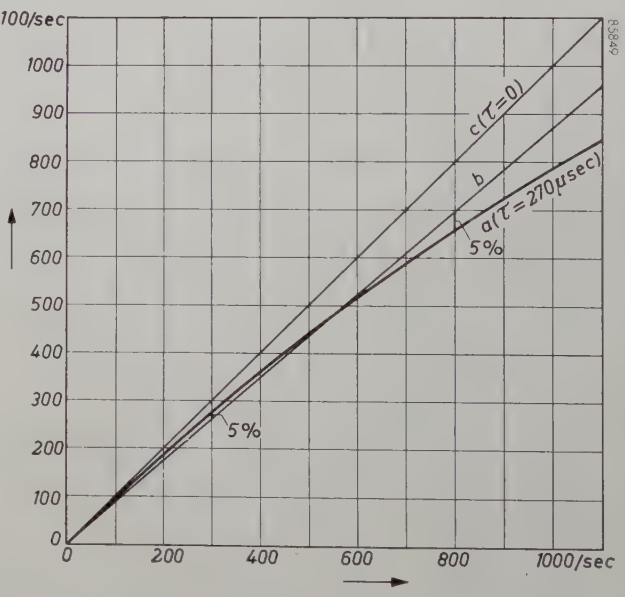

Fig. 19. Response (a) of the Geiger counter tube to random quanta as a function of the true average count rate. The deviation from linearity is due to the finite resolving time for successive quanta. The measured effective "dead time" of the "Norelco" No. 62019 Geiger counter is $\tau = 270$ μ sec for Cu Kα radiation from an X-ray tube operated with full wave rectification at 35 kV peak. With the X-ray tube operated at constant potential a smaller effective dead time is found; cf. note [15]). For $\tau = 0$, the straight line c would be obtained.

[13]) W. Parrish and A. J. C. Wilson, Precision measurement of lattice parameters of polycrystalline specimens, International Tables for X-ray Crystallography, Vol. II, in press.

[14]) Philips tech. Rev. **10**, 1-12, 1948/49.

[15]) The effective resolving time of the Geiger counter is longer than its true resolving time owing to the unfavorable bunching of the quanta: CuK radiation is produced only during a portion of the time, viz., whenever the undulating voltage exceeds the 8.8 kV excitation potential of Cu.

curve (*a*), or eq. (7), which are valid up to about $n = 1500$ counts/sec, can be used for correcting individual counting rates. When no corrections are made and a linear response is assumed, the straight line (*b*) drawn through the measured response curve in fig. 19 shows that the error is less than $\pm$ 5% for intensities whose observed counting rate is below 800 counts/sec.

New radiation detectors have been developed recently for use with the "Norelco" diffractometer, viz., the proportional counter and the scintillation counter [16]). Both have been designed in such a way that they can be substituted for the Geiger counter tube by the mere plugging-in of detectors and amplifier stages. (The lowest two panels of the rack shown in fig. 1 are used in conjunction with these detectors.) Both the new detectors have resolving times so short that the linearity of the counting system is limited principally by the dead time of the scaling circuit, which in the "Norelco" equipment is about 7 μsec. In this case, the deviation from linearity is 0.7% at an observed counting rate of 1000 counts/sec.

In applying the Cooke-Yarborough method, non-linearity is enhanced by the additional counting losses caused by the added pulses. Calculation of the largest loss, occurring at the highest added pulse frequency (240/sec), showed that with the 7 μsec resolving time, the deviation from linearity at $n = 1000$ counts/sec is increased only to 0.9%.

Specimen and X-ray source errors

To conclude this article, we should further qualify the statement that either the measured peak height of a diffraction line or its area will

[16]) J. Taylor and W. Parrish, Absorption and counting efficiency data for X-ray detectors, Rev. sci. Instr. **26**, 367-373, 1955 (No. 4).

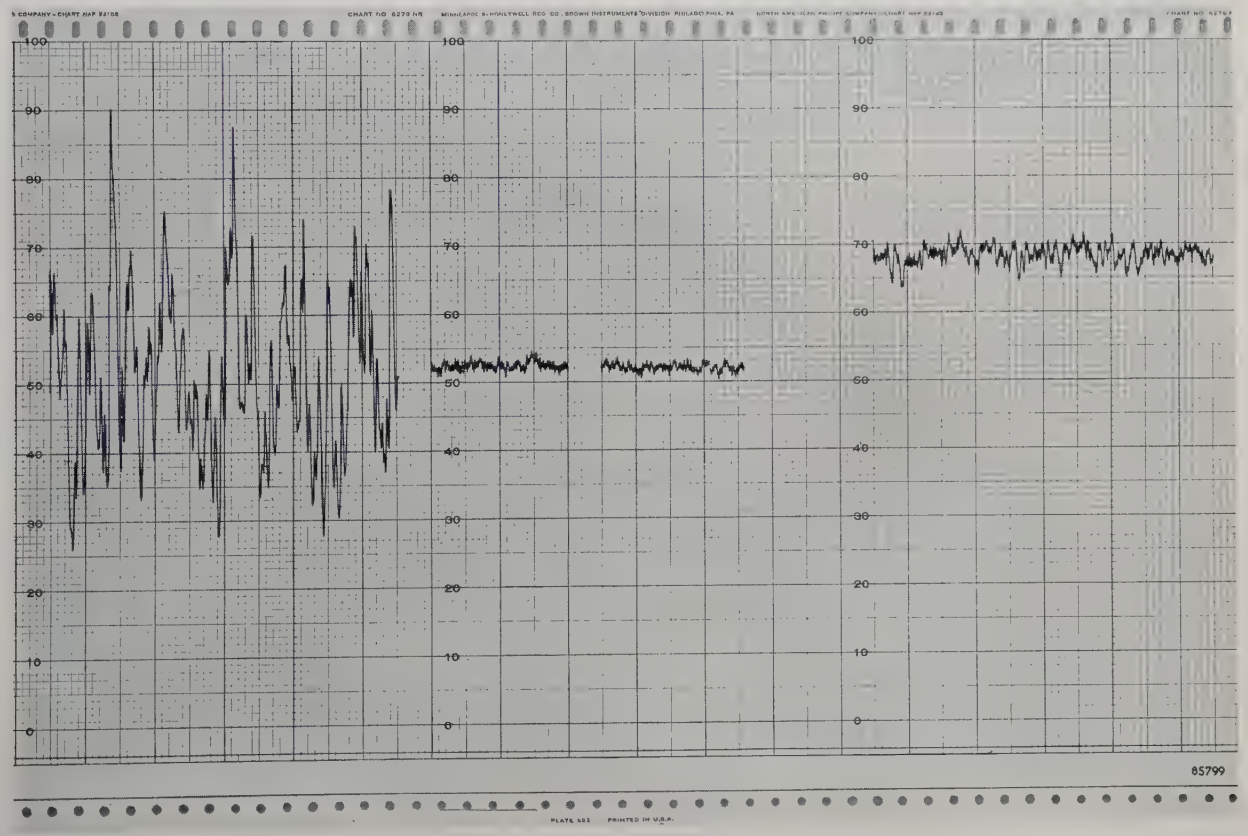

Fig. 20. *a*) Changes in diffracted X-ray intensity recorded at a fixed Bragg angle position of the detector when a specimen consisting of relatively large crystallites (30 - 50 μ) is slowly ($^1/_7$ rev/min) and continuously rotated in its own plane; silicon 111 line with Cu Kα radiation. *b*) By *rapid* rotation of the same specimen in its own plane (77 rev/min) the large intensity changes are averaged out. The remaining fluctuations are similar to those obtained with a stationary specimen (*c*). (The latter recording was made with a position of the specimen selected to give the same average intensity as obtained in *b*.) *d*) Slow rotation of a specimen with a much larger number of crystallites (size 0 — 5 μ) shows only small variations of intensity. (The 0-5 μ particles give a higher average intensity than the 30 - 50 μ particles probably owing to closer packing of the surface of the former specimen.)

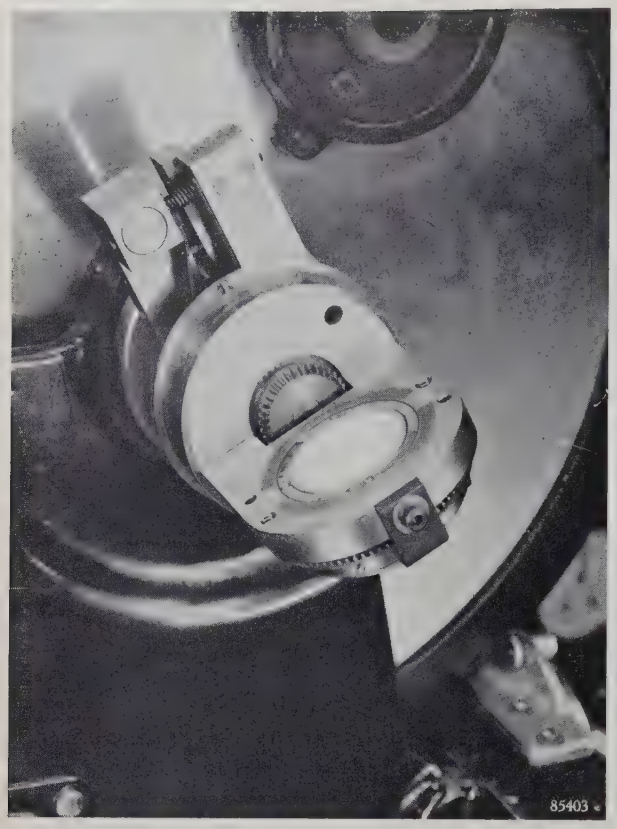

Fig. 21. Device developed by K. Lowitzsch of the Irvington Laboratory for rotating the specimen in its own plane.

offer a reliable indication of the concentration or of structural characteristics of a substance. Even if errors in the alignment of the goniometer or positioning of the specimen are disregarded (they do not greatly affect the integrated intensity of a line) the above statement will be true only for an ideal specimen. Preferred orientation, for example, should be entirely avoided, and the number of crystallites should be large enough for every possible reflecting position to be adequately represented. If there are too few crystallites, large fluctuations in diffracted intensity may be found in a fixed goniometer position when the flat specimen is slowly rotated in its own plane (*fig. 20a*). The remedy for this effect is to average out these fluctuations by *rapidly* rotating the specimen in its own plane during the measurements (fig. 20*b*). An accessory apparatus designed for the purpose (flat specimen spinner) is shown in *fig. 21*. Spinning the specimen, of course, will not generally eliminate errors due to a preferred orientation of crystallites. Because of the difficulty of preparing specimens entirely free of preferred orientation, an accuracy of 1% of the intensity measurements is therefore usually sufficient.

This 1% is actually also the long-time variation of the intensity of the X-ray source provided for the "Norelco" diffractometer. In cases where specimen conditions warrant a higher accuracy, it will be necessary to re-adjust the slowly varying X-ray intensity during one recording; this readjustment can be made in a simple manner by inserting a standard specimen and adjusting the X-ray tube current to give a prescribed counting rate for a given diffraction line. An X-ray source having a long-time stability better than 1% (PW 1010) is provided with the version of the diffractometer made by Philips in Europe.

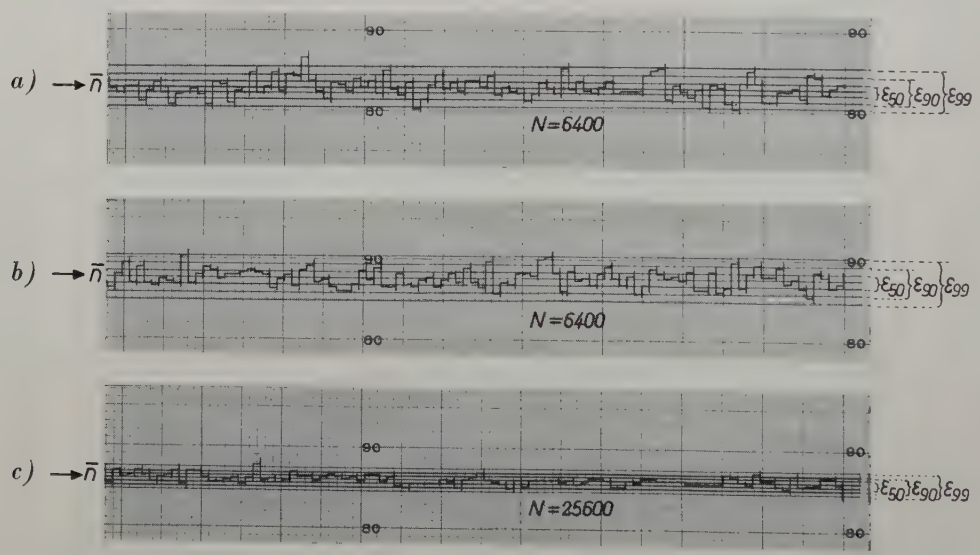

Fig. 22. Measurements of a constant X-ray intensity with the counting-rate computer, in order to check the statistical fluctuations of the counting rate. In each of the three cases, 100 measurements of a fixed number N of counts are performed.
a) Diffracted X-ray beam from a Cr-target, 13 kV peak, full wave rectification. $N = 6400$.
b) X-radiation from a radioactive source. $N = 6400$.
c) Diffracted X-ray beam from a Cr-target, 37 kV peak, full wave rectification. $N = 25\,600$.

Appendix: Statistics of X-ray quanta

The standard deviation $\sigma = \sqrt{N}$ (eq. 2) is valid for counting experiments performed on ideally random sequences of quanta (the results show a practically Gaussian distribution). In many cases the X-ray quanta are not produced at a strictly random rate, since the tube is not operated at constant potential but on a half or full-wave rectified voltage. Moreover the random sequence is marred to some extent by the finite resolving time of the counter tube and circuits. For a correct assessment of the accuracy obtained in the intensity measurements it is therefore important to check whether formula (2) is applicable to these measurements.

For a rough check, recordings involving 100 scanning steps with the counting rate computer have been made *a*) of a diffracted X-ray beam (Cr-target, 13 kV peak), with $N = 6400$; *b*) of the X-radiation of a radioactive source (where the quanta are emitted at a strictly random rate), with $N = 6400$; *c*) of a diffracted X-ray beam (Cr-target, 37 kV peak), with $N = 25\,600$. The recordings are shown in *fig. 22*. In fig. 22*a* and *b* according to eqs. (3), (3a), (3b), 50 steps should deviate less than $\varepsilon_{50} = 0.84\%$ from the average height, 90 steps less than $\varepsilon_{90} = 2.06\%$ and 99 steps less than $\varepsilon_{99} = 3.22\%$. The real numbers of steps found within these limits were 51, 78 and 97 for the X-ray tube and 42, 90 and 99 for the radioactive source. In fig. 22*c* the corresponding numbers of steps found within ε_{50}, ε_{90} and ε_{99} are 51, 91 and 99. These numbers agree reasonably well with the theory, although one number (78) is found which deviates from the theoretical number rather more than might be expected — from statistical considerations — in 3 groups of 100 measurements. However, a much larger number of measurements would be necessary to make sure whether significant deviations really occur.

Summary. In X-ray diffractometry the measurement of X-ray intensities is achieved by counting quanta with a radiation detector such as the Geiger counter, proportional counter or scintillation counter. The counting rate is computed from the number of counts (which is subject to a statistical error) and the counting time interval. Different systems of "counting strategy" are discussed. Counting during a fixed time at every Bragg angle position of the detector will yield a relative statistical error inversely proportional to the square root of the counting rate, whereas measuring the time necessary for a fixed number of counts will make the relative statistical error independent of the counting rate. A third possibility, yielding a constant absolute error in the counting rates, is also mentioned. The recording counting-rate meter and the counting-rate computer, being part of the "Norelco" X-ray diffractometer equipment, are described as representatives of the fixed time and fixed count methods. Facilities can also be provided for the Cooke-Yarborough method, which is a compromise between both methods. For precise quantitative chemical and structural analysis, the integrated intensities of diffraction lines have to be determined. Corrections for non-linearity of the intensity measurements caused by the dead time of the detectors (counting losses) are discussed. The influence of inadequate crystallite orientation in the specimen can be eliminated by spinning the specimen in its own plane.

FUNGICIDE RESEARCH

by M. J. KOOPMANS *).

632.952

Many agents are known for the control of fungus infections in cultivated plants, but apart from their specific useful properties, all have disadvantages of one sort or another. An active search for new agents is therefore in progress in many parts of the world — including Boekesteyn). This, the third article in the series on the work of this laboratory, gives a description of the research in the field of fungous control.*

General properties of fungi

Research relating to agents for controlling animal and vegetable pests in agriculture and horticulture is among the most important work carried out in the Boekesteyn Agrobiological Laboratory of N.V. Philips-Roxane. A review of this work has already been given in an introductory article [1]), and a second article was specially devoted to the combating of animal pests [2]). We now wish to discuss measures against another danger to which cultivated plants are exposed, namely, attack by the lower-organized plant organisms, known as fungi.

The losses ensuing from attack by fungi may be very appreciable. Thus in the United States annual harvest losses amounting to 2000 million dollars still occur as a consequence of inadequate control of fungous diseases. In tropical regions, a constant crop loss of 30% for such plants as banana, coffee and cocoa is by no means exceptional. In countries for which less dramatic figures can be reported it often happens that only the unceasing application of preventive measures keeps fungous infections within limits.

It is beyond the scope of this article to give a survey even of the most important fungal diseases, but it may nevertheless be useful to try to describe the general properties of these injurious organisms.

Many pathogenic fungi are propagated by their wind-borne spores. Examples are the rust fungus on wheat and the mildew mould on grapes, fruit trees, cereals, etc. Other fungi are propagated by splattering raindrops which carry away their spores, as is the case in scab on fruit and late blight in potato. In general both these groups cause leaf and fruit diseases.

Further, there are species whose spores adhere to the seeds of the host, so that the young plant carries the disease germs with it from the outset. We may cite in this category: bunt in wheat, black leg in beets and various diseases in peas.

Finally there is yet another category of plant-pathogenic fungi, whose members live in the soil and principally affect seedlings, although the symptoms of the disease may only become manifest at a later stage in the life of the plant. Some important crops which are prone to attack as seedlings, are beets, cucumbers and peas.

The vast majority of plant-pathogenic fungi thrive at high temperatures (24 °C) and in humid atmospheres. That is why fungous diseases constitute such a serious problem in the tropics. On the other hand, infection is a matter not only of the virulence of the fungus, but also of the power of resistance of the plant, and it may thus so happen that it is precisely low temperatures which promote infection of the plant. This is particularly true of soil fungi which cause diseases in seedlings.

Review of existing fungicides

Agents which protect plants against fungous diseases, are called fungicides. In the majority of cases their action is prophylactic, that is to say their presence precludes infection: the germination of the fungal spores is prevented. Actual cure of the plant, in the sense that an infection which has already developed, is driven out, or even merely checked, is practically never found in the control of fungal diseases. This problem will be broached from another angle in a subsequent article.

Besides their unmistakable advantages, various known fungicides have serious disadvantages. Thus lime sulphur (calcium polysulphide [23] [3]), which has been in use since 1888 for controlling, inter alia, scab in fruit trees, is a good fungicide, but it unfavourably influences the development of the trees and the appearance of the fruit to such an

*) Boekesteyn Agrobiological Laboratory, N. V. Philips-Roxane, 's-Gravenland, Holland.

[1]) R. van der Veen, Philips tech. Rev. **16**, 353-359, 1954/55 (No. 12).

[2]) J. Meltzer, Philips tech. Rev. **17**, 146-152, 1955/56 (No. 5).

[3]) The numbers in square brackets refer to the structural formulae in the appendix. The numbering follows on from that of the previous articles [1]) and [2]).

extent that it is in fact no longer used at the present time for the new varieties. More recent preparations, such as colloidal sulphur and the organic sulphur compounds thiram [1], zineb [2] and captan [5] [4]) are welcome successors. The latter even has a positive effect on the appearance of the fruit, enhancing its colour and sheen.

Copper in the form of Bordeaux mixture (basic copper sulphate [24], and the related copper oxychloride [25], is still a very popular fungicide, although it has been in use since 1882. For combating numerous diseases it still does excellent duty, but nevertheless, in many cases, a substitute is readily accepted. In many varieties of fruit, spraying with copper gives rise to undesirable russeting; in ornamental plants the bluish-green colour of the deposit is disadvantageous, and added to this the leaves are frequently damaged. As a result, Bordeaux mixture has found competitors in zineb and captan. Zineb has certain advantages over copper, since plants sprayed with it retain their greeness longer, this leading in many cases to a greater crop. Zineb adheres less tenaciously to the plant (see below) than copper however, as a result of which the protection may be of shorter duration.

The excellent fungicidal properties of the organic mercury compounds, which have also been used for many years, go hand in hand with a powerful leaf-damaging action and a high toxicity to warm-blooded animals. Thus an intensive search is in progress for substitutes for this group.

For various fungous diseases — mildew in apple trees for example — no satisfactory combating agent has yet been found. Here then is a virgin field for the development of new preparations. This and the above-mentioned defects of existing fungicides are the reasons for the current large-scale search for new fungicides.

Properties to be considered in fungicide research

According to the form in which they will be used, the control agents sought may be divided into the following four groups:

a) Wettable powders, i.e. preparations which may be readily suspended in water and, with the aid of this vehicle, may be sprayed over the plant.

b) Dustable powders, i.e. mixtures of an active component with inert carrier powders, which can be dusted over the plant. Agents (*a*) and (*b*) find application in combating leaf and fruit diseases.

c) Dry powder preparations to disinfect sowing-seed, which are mixed in a small percentage with the seed. They kill the fungal spores on or in the seeds and protect the seedling against soil fungi.

d) Soil treatment agents, which, mixed with the top-soil, serve to combat the sources of root and seedling diseases.

Irrespective of the final form of the fungicide, a large number of factors must always be taken into account in deciding its composition. A number of these factors are cited in random order below:

1) Fungicidal activity of the active component; by this is meant the intrinsic fungus-killing power of the compound. This power must of course conform to a certain minimum requirement.
2) Resistance of the preparation to external influences (moisture, temperature, light). This can never be too great.
3) Solubility of the active component. There is an optimum value: if the solubility be too low the toxic concentration cannot be reached and there will thus be no fungicidal action; if it be too high the fungicide will be washed away too rapidly.
4) Adhesion of the preparation once it has been applied to the leaf: the better the adhesion, the more slowly the fungicide will be washed away by rain or dew.
5) Distribution of the preparation over the plant. One factor determining this is the wetting agent content. Here too there is an optimum value: too little wetting agent gives poor distribution, too much leads to loss by draining.

The experiments relating to fungicide research conducted in the Mycological department at Boekesteyn can be divided into two categories. In the first only one living organism is involved, for example the spores or the mycelium [5]) of a fungus, and the action of a preparation is judged by the extent to which it is able to prevent the germination of the spores or the growth of the mycelium. The second category involves two living organisms, namely, both the disease-producing fungus and a host that has been artificially infected. We shall now discuss these two categories more closely.

---

[4]) Thiram, captan, etc., are names of two or three syllables, usually derived from the initial letters of some of the components and used by mutual agreement to replace complex chemical descriptions. Such names are coined only when an agent has shown that it is going to assume some practical significance.

[5]) Mycelium is the thread-like or fluffy vegetative part of a fungus.

Experiments involving one living organism

The spore germination test

For determining fungicidal activities under glass, use is often made of the spore germination test. In principle the test is performed as follows. A series of diluted solutions in acetone are prepared from the compound under investigation, and a known number of 0.01 millilitre drops of each solution are placed on a glass slide (*fig. 1*) with the aid

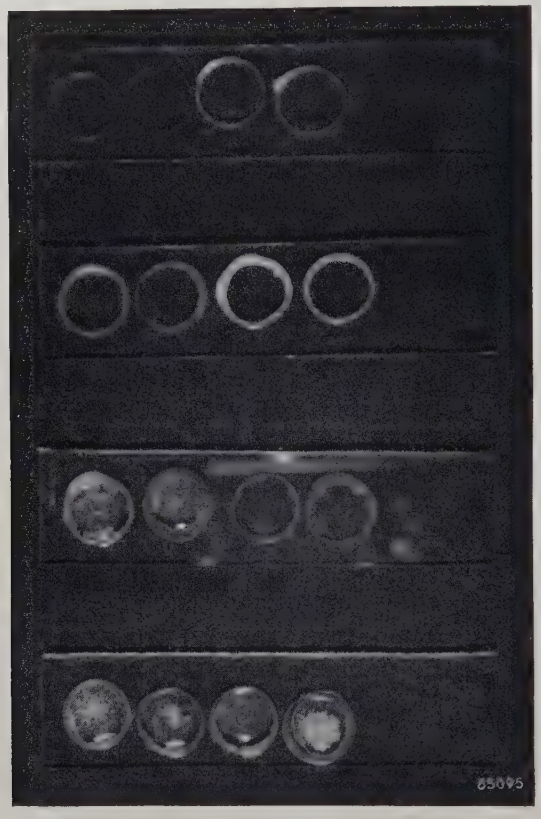

Fig. 1. Germination slides, with small paraffin wax rings, into which a known amount of the compound to be investigated and a drop of an aqueous suspension of the fungal spores are introduced.

of a micro syringe which permits of very accurate dispensing. To ensure that the solution is distributed over a known area, paraffin wax rings are placed on the glass slide. When the solvent has evaporated off, a known amount of the compound under investigation is left behind within each ring in the form of a more or less uniform layer. An 0.05 ml drop of an aqueous suspension of fungal spores (usually those of Fusarium culmorum, *fig. 2a*) is then placed on this layer. A little cherry extract is added to the suspension to render the environment favourable for the subsequent germination process. The glass slides are then placed in tubular containers, which are closed with a plate covered with moist filter paper (*fig. 3*). After a period of about 20 hours at 20 °C, it is ascertained whether or not the spores have germinated (fig. 2).

It would take us too far from our subject to discuss the spore germination test in detail. It will suffice to say that the concentration that is just able to suppress the germination of the spores completely or almost completely, is usually taken as a measure of the fungicidal activity of the compound. Use is made of a concentration series in which each solution of fungicide is of half the strength of the next highest. If greater accuracy is required, as for example in standardizing a preparation, then the dilution steps must lie closer together and the percentage germination must be determined for each of the dilutions, so that an "LD50" may be arrived at; LD50 is the designation given to the concentration which is lethal to 50% of the individual spores (LD = lethal dose). This value is obtained by determining the percentage germination for each solution of the concentration series used, and analysing the results graphically. Investigation in this manner is more accurate than the former method but requires a great deal of time, since it necessitates the individual examination of a large number of spores.

The spore germination test can equally well be employed for compounds which are soluble in water or can be suspended in it. The concentration series are prepared, using the spore suspension as diluent, and 0.05 ml drops of the various concentrations (which thus already contain the spores) are measured out onto the germination slides.

The spore germination test is essentially an analytical method. It may be used not only to determine the fungicidal value of unknown compounds, but can be adopted as means of establishing the content of a known fungicide. So employed, the spore germination test forms the cornerstone of research relating to resistance and adhesion (see below), and preparations of unknown composition can be analysed with it, provided the nature of their active component is known. Generally speaking the spore germination test can be said to be an aid to the search for new combating agents and better "formulations" (i.e. the form in which the compound is used: dusting powder, spray, etc).

Investigation of the effect of soil organisms

The extent to which fungicides are decomposed by soil organisms is investigated in the following manner. The compounds are mixed with soil rich in humus and the mixture allowed to stand for several weeks under conditions of humidity, oxygen

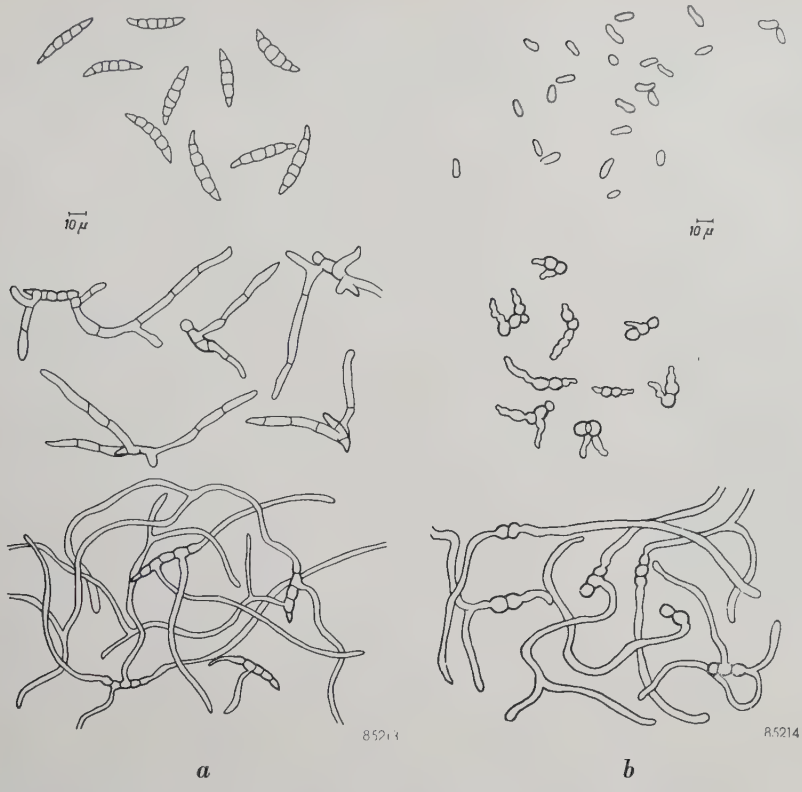

Fig. 2. *a*) Ungerminated spores (above), germinated spores (centre) and further mycelium growth, of the fungus Fusarium culmorum. (*b*) The same for the fungus Mycosphaerella pinodes.

supply and at the temperature (24 °C) that is optimum for the development of the microflora. The compounds are then extracted with acetone or another solvent, and the activity of the extract is determined by means of the spore germination test. For the purpose of eliminating secondary influences of the soil (adsorption, activity of soil components) a determination is always carried out on a mixture of the soil with the compound under investigation, immediately after this mixture has been prepared.

Determination of the sticking power

A method for the determination of the tenacity or sticking power of the preparations should also be mentioned. Samples introduced onto spore germination slides are exposed to an artificial rainfall of 1 cm per hour, in the apparatus shown in *fig. 4*. *Fig. 5* shows the working

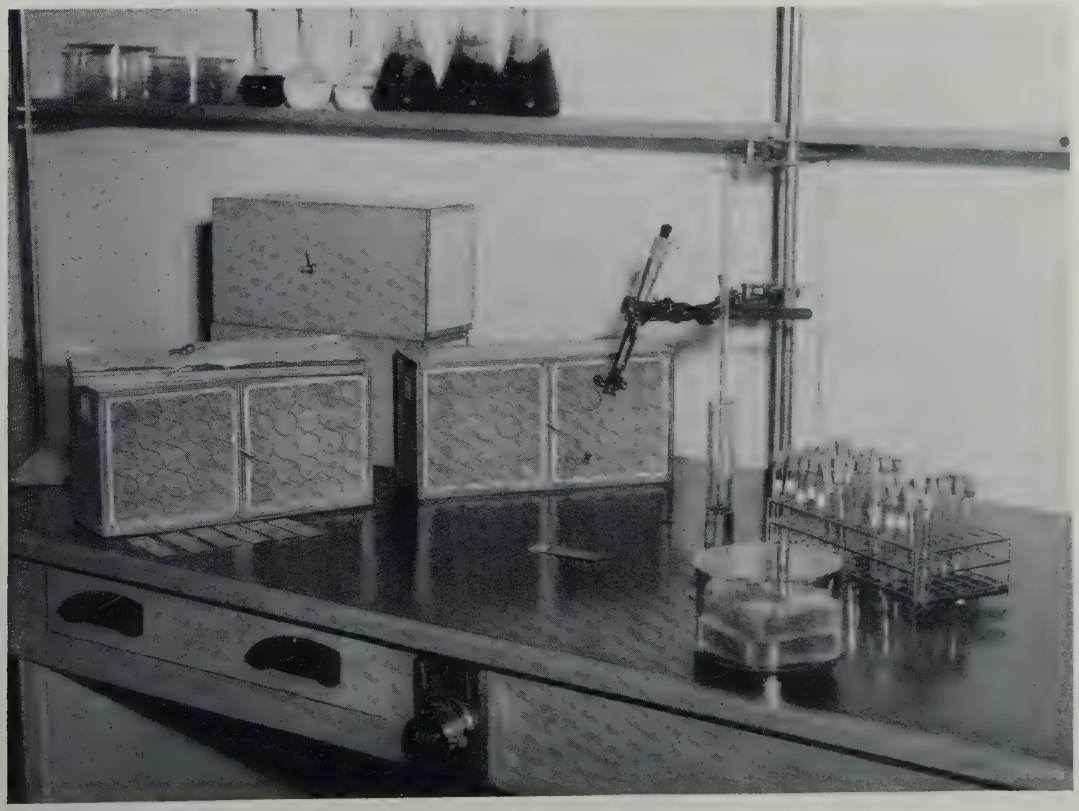

Fig. 3. The germination slides are inserted into glass cylinders (left), whose ends are covered with moist filter paper, Right: test tubes containing fungal suspensions; in the centre: micro syringe for accurate dispensing.

Fig. 4. An apparatus for determining the extent to which fungicidal preparations remain fixed to glass during rainfall.

principle. After 1 to 2 hours of rain, the fungicidal activity of the layers on the slides is compared with that of layers on slides which have not been exposed to rain. The values of the sticking power found in this way are compared with those of standard preparations.

The sticking power is also determined with leaves (e.g. potato leaves, see below) as the sub-surface; here the protective action of the fungicide against a subsequently applied artificial leaf infection serves as the yardstick. Experiments of this kind belong to the second category (two living organisms).

Investigation of the effect of toxicants on the growth of mycelium

In some cases it is desired to examine the influence of a toxicant on the growth of mycelium. A method is available for this purpose, which makes use of so-called notched tubes. A notched tube is a culture tube with an indentation just behind the mouth, which enables an agar culture medium to set in a layer parallel to the longitudinal axis (*fig. 6*). The culture medium is mixed beforehand with the compound to be investigated. A piece of mycelium from the fungus is placed in the centre of the agar layer. After a time (5 to 20 days depending upon the species), the spread of the mycelium is determined by comparison with a control experiment.

Investigation of bactericidal activity

In some cases an investigation is made of the bactericidal activity of new compounds. Use is made here of a score of plant-pathogenic bacteria. The experiment is the same as the spore germination test, save that a culture medium favourable for bacteria is used and the criteria by which the test is judged are "growth" (solution becomes turbid) and "no growth" (solution remains clear).

Experiments involving two living organisms

The second category of experiments for determining the fungicidal activity of preparations, namely that in which a host is artificially infected with a disease-producing fungus, approximates more closely to actual practice than the first. Nevertheless the second category is still a laboratory method, in which many factors obtaining in practice (rain, irradiation by the sun, wind, nature of the soil, manuring, irrigation, etc) are deliberately eliminated or standardized.

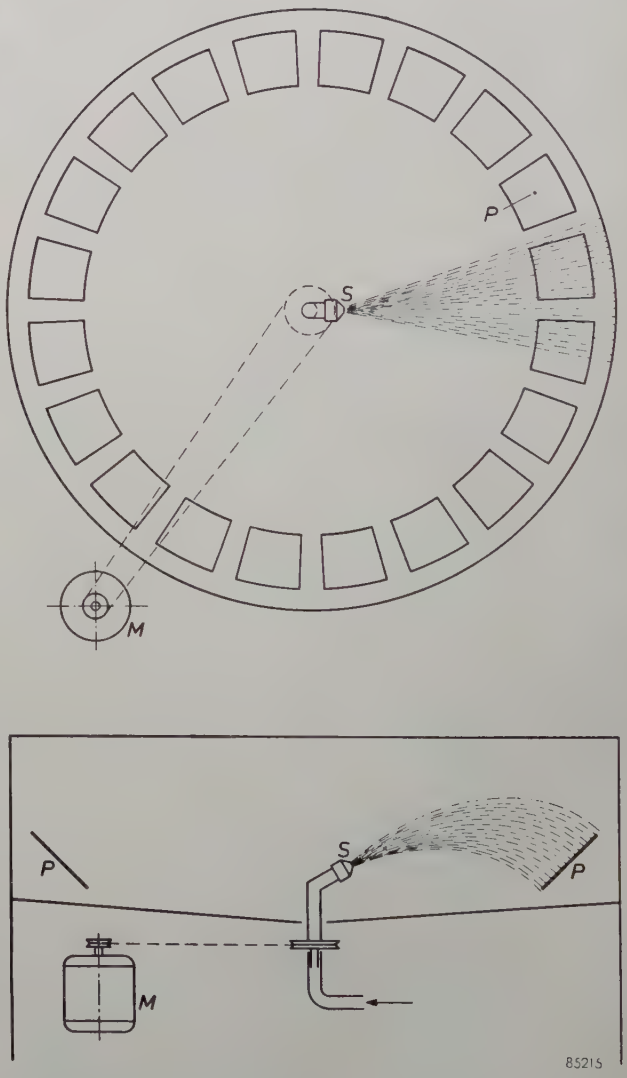

Fig. 5. The apparatus in fig. 4 is seen from above and in section. The sprayer S is rotated about a vertical axis by an electric motor M, and plays successively on the glass slides P which have been treated with the preparations whose sticking power is to be investigated. A rainfall of 1 cm per hour is employed for a period of 1 to 2 hours.

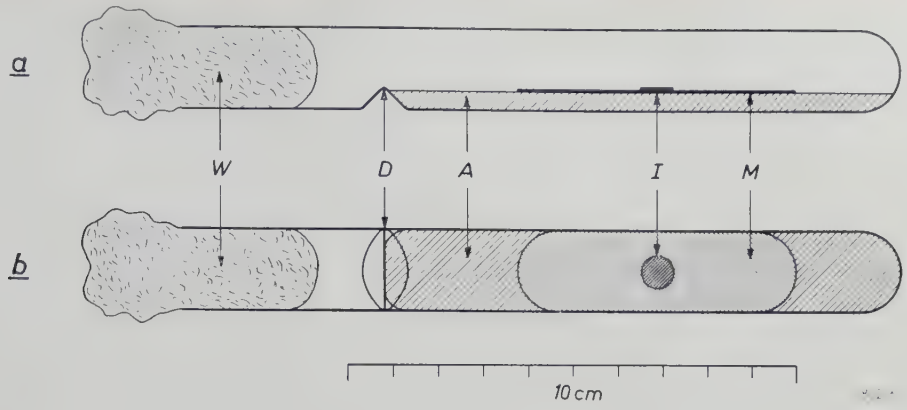

Fig. 6. Notched tube (*a*, seen from the side, *b* from above), with indentation *D*. *A* agar culture medium, mixed with the compound under investigation. *I* inoculum (piece of mycelium from the fungus). *W* cotton-wool plug. After a certain time the spread *M* of the mycelium is compared with that of a control test.

Experiments involving artificial infection usually take the following form. The plants (or parts of the plants) are sprayed with a spore suspension (with a density of the order of 100 000 spores per millilitre), or dusted with air-dried spores (in the case of powdery mildew). The plants are then placed for 24 hours in a room in which the relative humidity is always near 100% and at the optimum temperature for germination and the infection process (usually around 20 °C for the species used). This gives the disease opportunity to establish itself. The plants are then transferred to an environment favourable for the disease to develop. The temperature varies according to the species between 18 and 25 °C, a relative humidity of 75% will generally suffice, and in addition care must be taken that there is adequate lighting, so that the conditions are favourable for the development of the plant.

Fig. 7. Leaves from a young barley plant. Left to right: healthy leaf, leaf lightly attacked and leaf severely attacked by a species of powdery mildew (in this case Erysiphe graminis).

Fig. 8. Left: leaves of a young pea plant attacked by Mycosphaerella pinodes (fig. 2*b*). Right: healthy leaves.

The protective action of fungicide preparations is now investigated by starting from plants that prior to infection have been sprayed with the compound to be examined. It is then observed that the degree in which the symptoms of the disease occur, depends upon the concentration of the fungicide that had been applied to the plant.

Fig. 9. Tomato leaves infected with Phytophthora infestans. From left to right: untreated plant, plants treated with 0.2%, 1% and 5% copper oxychloride [25].

A number of plant diseases are currently employed for this purpose. We cite the following:

a) Young barley plants (about 8 cm tall) begin to show small white powdery specks about five days after infection, as a result of the development of the spores of powdery mildew (Erysiphe graminis), see *fig. 7*.

of the familiar late blight. The leaves shrivel, and if the humidity of the air be sufficiently high, become covered with a white fluff of mycelium.

d) Tomato plants (cut leaves or young plants) infected with Phytophthora infestans show a similar picture (*fig. 9*).

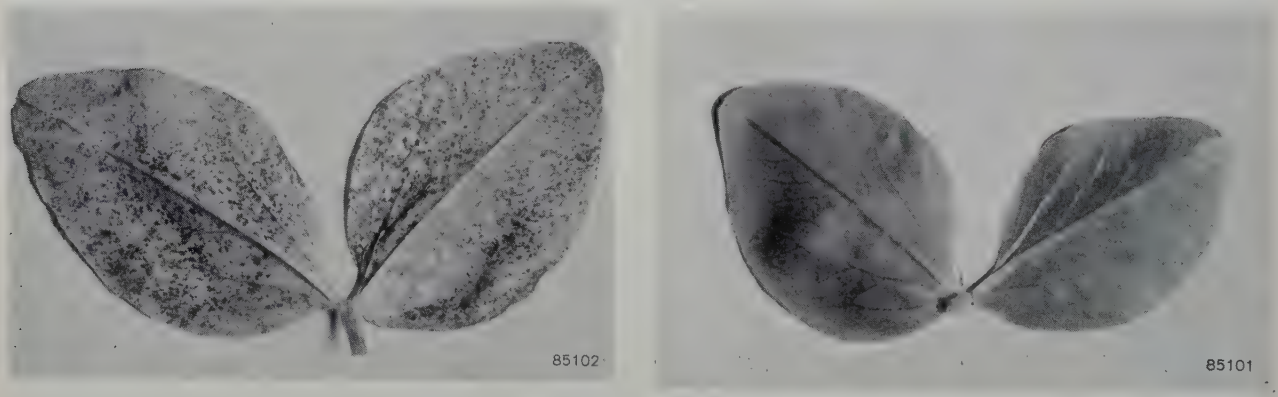

Fig. 10. Broad-bean leaves, left: infected with Botrytis fabae, right: healthy.

b) Young pea plants (also about 8 cm tall), sprayed with the spores of Mycosphaerella pinodes (fig. 2*b*), are covered after a few days with brown flecks (*fig. 8*).

c) Leaves cut from the potato plant, with their stems placed in water, die within five days of having been artifically infected with the spores of Phytophthora infestans, the causative organism

e) Another favourite infection is chocolate leaf spot in broad-beans. Within about two days, the causative fungus (Botrytis fabae) gives rise to round dark-brown spots on the broad-bean leaf, that stand out sharply against the somewhat greyish-green leaf (*fig. 10*).

f) The cucumber also shows disease symptoms when the young plants are treated with Colleto-

trichum lagenarium. After a few days, irregular, light-brown spots appear and finally the leaf completely withers.

In all infection tests, the activity of the preparation under investigation is expressed in terms of the activity of one or more standard preparations. Copper oxychloride, zineb and organic mercury preparations are some of the standards used.

If the provisional infection tests prove favourable, they are repeated, but this time with a practical preparation worked up from the compound. The results obtained serve as a pointer for the ultimate field tests, in which the efficacy is assayed in orchard, field, kitchen-garden or greenhouse.

Concluding remark

In the foregoing we have outlined the task of the Boekesteyn mycological department, as the link between chemical research and field tests. In general the work described has been the application of methods to be regarded as belonging to the routine work of the laboratory. Apart from this, however, investigations of a more fundamental nature are undertaken. Just recently, for example, a study of the penetration of substances (primarily fungicides) into the tissues of both fungi and the higher plants has been initiated. In this investigation, use is made of compounds labelled with radio-active isotopes. We hope that the results will give a better understanding of the mechanism of the leaf-damaging action of some fungicides.

APPENDIX: STRUCTURAL FORMULAE

Below are given the structural formulae of the compounds mentioned in the text.

Sulpher preparations

[1] Tetramethylthiuram disulphide (thiram, TMTD) . . . . . 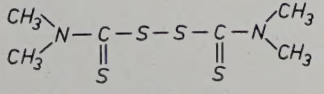

[2] Zinc ethylene bisdithiocarbaminate (zineb, dithane) . . . . . 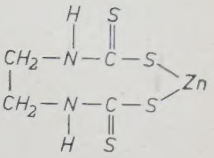

[5] N-trichloromethyl tetrahydrophthalimide (captan, orthocide) [6] 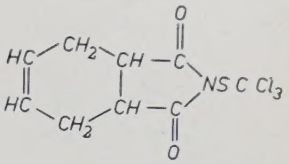

[23] Calcium polysulphide, the principal constituent of lime sulphur (The precise structure of this compound is still uncertain; one of the more recent ideas is given here.) . . . . . 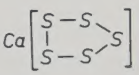

Copper preparations

[24] Basic copper sulphate (principal constituent of Bordeaux mixture) . . . . . $[Cu(OH)_2]_3CuSO_4$

[25] Copper oxychloride . . . . . $[Cu(OH)_2]_3CuCl_2$

Mercury preparations

[26] R-Hg-X, in which R is an aliphatic or aromatic group (preferably C_2H_5 or phenyl) and X an acid radical (usually Cl or phosphate, or an organic acid radical, such as p-toluene sulphonamide or dichlorocresol). Examples: ethyl mercury sulphide ("New Improved Ceresan"), phenyl mercury dichlorocresolate.

Summary. The principal task of the Boekesteyn mycological department of N.V. Philips-Roxane consists in the testing of compounds for their fungicidal action. This work forms a link between chemical research work and field tests. It may be divided into two categories. In the first, the only living organism involved is the fungus, whose reaction under glass to various dilutions on the compound under investigation is examined. The spore germination test (followed by descriptions of investigations of the influence of soil organisms, and on adhesion to the plant) and the investigation of the effect on the growth of the mycelium are discussed. The second category employs two living organisms: a fungus and a plant artificially infected with it. Besides this routine work the mycological department also undertakes research of a more fundamental nature, in which radio-active isotopes are employed to investigate the penetration of control agents.

---

[6]) In article [1]), page 358, an incorrect formula was given for this compound.

ABSTRACTS OF RECENT SCIENTIFIC PUBLICATIONS BY THE STAFF OF N.V. PHILIPS' GLOEILAMPENFABRIEKEN

Reprints of these papers not marked with an asterisk * can be obtained free of charge upon application to Philips Electrical Ltd., Century House, Shaftesbury Avenue, London W.C. 2.

2210: M. L. Huggins and J. M. Stevels: Comparison of two equations for calculation of densities of glasses from their compositions (J. Amer. Ceramic Soc. **37**, 474-479, 1954).

Two different relationships have been proposed by the authors, individually, for the calculation of the densities of glasses from their compositions. These relationships are here compared with regard to accuracy, composition limitations, relationships between their constants, etc. The Stevels equation is useful in supplying values (accurate to within about 2%) of the density of glasses having a high proportion of network formers (e.g., Si, B, and Al). Whether or not it is applicable, with different constants, when the content of network modifiers (e.g., Na, Ca, and Pb) is high, has not been determined. The Huggins relationship involves more empirical constants, including two which have different values, depending on which of four composition ranges is pertinent. It is considerably more accurate for well-annealed glasses of accurately known composition. Difficulties arise in applying it to glasses having a high content of network formers other than silicon or to glasses having components for which accurate values of the necessary constant have not previously been deduced. It is interesting to note that the limiting conditions of the Stevels equation lead, at least for the sodium silicate system, to the same breaks of the volume-concentration curves as found by Huggins. Comparison of the two relationships yields a better understanding of the reasons for the long-realized fact that the presence of certain elements, such as Li, Be, and Ti, invalidates the Stevels equation.

2211: W. P. van den Blink, E. H. Ettema and P. C. van der Willigen: A new proces of stud welding (British Welding J. **1**, 447-454, 1954).

A new process of stud welding is described, in which the timing is regulated by a cartridge on the end of the stud. This cartridge is a semi-conductor; it starts the arc between stud and plate, and also determines the distance between them. The composition of the cartridge resembles that of a normal electrode coating in so far as metallurgical and arc-stabilizing functions are concerned, and rimmed-steel studs and A.C. can be used. A simple stud-welding gun containing only a spring, pressing the studholder on to the work piece, can be used.

2212: P. J. L. Scholte, C. C. Kok van Alphen and B. Combée: Treatment of the cornea with a new lilliput roentgen tube (Acta Radiologica **42**, 316-328, 1954).

A description is given of a new lilliput X-ray tube energized at a potential of 25 kV and the basic principles of its design are discussed. Certain experiments carried out on the cornea of rabbits are reported and the results of treatment of the human cornea with the Philips 50 kV contact therapy apparatus and a 25 kV unit with the new tube are presented and commented upon. Both in "keratitis" and vascularisation of transplanted cornea, the results appeared to be most promising.

2213: M. E. Wise: The ratio of two factorials and some fundamental probabilities (Kon. Ned. Akad. Wet. Amsterdam **A 57**, 513-521, 1954).

Expansions are obtained for the ratio $N!/(N-n)!$ of two factorials, and for the logarithm of this ratio. It is shown how several well-known results in probability theory and statistical mechanics are thereby obtained much more easily than by the standard approach using Stirling's approximation for the factorials. In fact the latter seems to be even incorrect in one important case, viz. in finding how a binomial distribution approaches its limiting Gaussian form. Arising out of this, a new continuous probability function is found that is close to the binomial over its whole range, and may be useful in empirically fitting some observed distributions when it is important to estimate their behaviour accurately at the tails (i.e. extreme values).

2214: Th. A. J. Payens: Influence of salt on the spreading pressure of films of long-chain weak acids (Kon. Ned. Akad. Wet. Amsterdam **B 57**, 529-533, 1954).

The ionization of incompletely ionized monolayers at an air-water or oil-water interface depends not only on the ionization constant of the monolayer electrolyte but also on the electrical potential at the interface. As a consequence, the surface pressure of long-chain weak electrolytes may be increased by other ionizing substances, such as salt, dissolved in the water. Experimental evidence of this is presented with monolayers of stearyl phosphoric acid

at an oil-water interface and with caprylic acid at an air-water interface.

2215: J. W. L. Köhler and C. O. Jonkers: De koudgaskoelmachine (De Ingenieur **66**, 0 103-0 110, 1954). (The gas refrigerating machine; in Dutch).

See Philips tech. Rev. **16**, 69-78 and 105-115, 1954/1955.

2216: J. L. H. Jonker: Secondary emission (T. Ned. Radiogenootschap **19**, 267-281, 1954).

The following principal properties of secondary emission are dealt with: the secondary emission of metals, the secondary emission of insulators, secondary emission as a function of the angle of incidence of the primary electrons, the energy distribution of the secondary electrons, and the angular distribution of the secondary electrons. Some properties can be qualitatively understood by means of a simple classical theory. At the end some conditions for practical application of the secondary emission of metals, insulators and semi-conductors are discussed.

R 261: J. Bruijsten: Graphical determination of reflex-klystron characteristics (Philips Res. Rep. **10**, 81-96, 1955, No. 2).

The small-signal theory of reflex klystrons has been treated very thoroughly in literature. The article shows that some of the results obtained can be derived by a graphical method. Starting from an expression of normalized efficiency as a function of the bunching parameter, a triangular diagram is derived of normalized efficiency as a function of resonator loss conductance, load conductance and small-signal electronic conductance. This diagram can be applied for the construction of an electronic tuning diagram and a theoretical Rieke diagram. A method is described of evaluating the parameters from experimental data with the aid of the diagrams.

R 262: M. E. Wise: Formulae relating to single-sample inspection by attributes (Philips Res. Rep. **10**, 97-112, 1955, No. 2).

Operating characteristics (O.C.) for batch inspection by single attribute samples are considered; mathematical formulae for them are restated and used to derive accurate expressions for the 50-per-cent point of an O.C. and its slope at this point, and also some simple approximations which are compared with empirical ones. They are given both for infinite batches (with binomial distributions of the number of defectives found in a sample of n) and for finite ones (hypergeometric distributions). The general treatment of O.C.'s in terms of their behaviour at the 50-per-cent point is discussed. In a numerical example an attribute sampling system for a finite batch is given and an equivalent variable system is calculated; the two O.C.'s are compared.

R 263: J. Smit and H. G. Beljers: Ferromagnetic resonance absorption in $BaFe_{12}O_{10}$, a highly anisotropic crystal (Philips Res. Rep. **10**, 113-130, 1955, No. 2).

The ferromagnetic resonance absorption has been measured at 24 000 Mc/s for a single crystal of hexagonal $BaFe_{12}O_{19}$. The resonance conditions are severely influenced by the crystalline anisotropy and, for fields too small for saturation, also by the Weiss-domain structure. The theory predicts, for a varying magnetic field perpendicular to the hexagonal axis, at most three absorption peaks, which have been observed at elevated temperatures. The spectroscopic splitting factor g and the anisotropy field are evaluated. The g-factor has the spin-only value. The crystalline anisotropy is suggested to be caused by dipole-dipole interaction.

R 264: K. F. Niessen: Magnetic anisotropy and Van Vleck's relation for antiferromagnetics (Philips Res. Rep. **10**, 131-140, 1955, No. 2).

For the influence of magnetic anisotropy on the susceptibility of antiferromagnetics a formula (12) is derived which is more general than that given by Nagamiya, since anisotropy coefficients are supposed to be different for the two kinds of magnetic spins and also a small difference in the spin moments is taken into account. A corresponding extension (15) of Van Vleck's relation between the powder susceptibilities at 0 °K and at the Curie temperature is given.

R 265: T. Tol, W. J. Oosterkamp and J. Proper: Limits of detail perceptibility in radiology particularly when using the image intensifier (Philips Res. Rep. **10**, 141-157, 1955, No. 2).

Report in more detail of the investigation described in Philips tech. Rev. **17**, 71-77, 1955, No. 3.

R 266: H. Koelmans: Suspensions in non-aqueous media (Philips Res. Rep. **10**, 161-193, 1955, No. 3).

The stability of suspensions in solvents of very low dielectric constant ($\varepsilon<5$) is dealt with in the first three sections. Theoretical considerations lead

to the conclusion that quite modest electric charges and ζ-potentials are sufficient to stabilize suspensions of coarse particles (>1 μ), whereas hardly any stabilization can be expected from adsorbed layers of non-ionized surface-active molecules. Experiments on the setting-times of suspensions in xylene confirm that only ionized surfactants give rise to stability: detergents that do not increase the conductivity of the xylene do not give rise to a sufficient ζ-potential of the particles and do not improve the stability very much. The behaviour of suspensions in polar organic media is dealt with in the fourth and fifth sections, in relation to the phenomenon of electrophoretic deposition. It is shown that the particles are accumulated near the electrode by the applied field, but that the formation of an adhering deposit is caused by flocculation, introduced by the electrolyte formed as a result of the electrode reaction.

R 267: G. Diemer: Light patterns in electroluminescent ZnS single crystals activated by diffusion of Cu (Philips Res. Rep. **10**, 194-204, 1955, No. 3).

Non-activated ZnS single crystals can be made electroluminescent by providing them with copper electrodes through evaporation in vacuum. It is shown that at temperatures little above room temperature the copper diffuses rapidly along the surface of the crystal and along certain imperfections into the bulk of the crystal. During electroluminescence in an a.c. field, light is emitted only from narrow lines, which with high optical magnification prove to consist of a series of nearly equidistant dots. These "dotted lines of light" always have the same direction as the main direction of growth of the hexagonal crystals.

R 268: P. Zalm, G. Diemer and H. A. Klasens: Some aspects of the voltage and frequency dependence of electroluminescent zinc sulphide (Philips Res. Rep. **10**, 205-215, 1955, No. 3).

Experiment shows that the relation between the luminous emittance H of an electroluminescent cell and the applied r.m.s. voltage V is given by $H = H_0 \exp(-c/V^{\frac{1}{2}})$. A mechanism is proposed that may explain both the well-known linear frequency dependence of the emittance at constant r.m.s. voltage and the observed voltage dependence.

R 269: G. Thirup: Design of low-pass amplifiers for fast transients (Philips Res. Rep. **10**, 216-230, 1955, No. 3).

By means of network synthesis a broad-band amplifier is designed, special attention being paid to a good transient response. The design leads to a novel type of interstage network. Some details of a 50 Mc/s amplifier are given: measured phase and amplitude curves as well as transient response are shown. In an appendix details of the design of the phase-correction network are given.

R 270: P. Schagen: Limiting resolution due to charge leakage in the scenioscope, a new television-camera tube (Philips Res. Rep. **10**, 231-238, 1955, No. 3).

The conductivity of the target material in the scenioscope, a new television pick-up tube, results in leakage of picture charge through the target. The potential distribution at the surface of the target between successive scans is calculated for the case where picture charge is supplied to the target on alternate illuminated and dark bars with a width d. The potential difference between the centre of illuminated and dark bars immediately before the next stabilization by the scanning beam appears to be a function of τ/R_0C_0 (where τ represents the frame period and R_0C_0 the RC-time of the target material) and of the relative picture detail d/D, where D is the target thickness. Formulae are derived for two effects of the target characteristics on the picture signal: (1) Leakage of picture charge to the signal plate results in a loss of sensitivity, determined by τ/R_0C_0. (2) Leakage of picture charge parallel to the surface of the target results in a decreased depth of modulation for smaller picture details d/D. Limiting values for τ/R_0C_0 and d/D follow from the requirement of a negligible influence of these two effects.